

COULOMB EXCITATION OF ^{140}Sm

by

Trond Wiggo Johansen

THESIS

for the degree of

MASTER OF SCIENCE



Faculty of Mathematics and Natural Sciences
University of Oslo

September 2019

Abstract

To my family, for all their support and encouragement!

Acknowledgements

Supervisors Professor Andreas Görgen and Dr. Katarzyna Hadyńska-Klęk
Nuclear Physics Group
Computational Physics Group, Professor Morten Hjorth-Jensen
CERN-ISOLDE, Dr. Liam Gaffney
Ville Virtanen from University of Jyväskylä for tips on scripts.
Lillefy, FFU, Fysikkforeningen
My family
Morten, Alex and Astrid.
Ina, for pushing me towards excellence, I love you.

Collaboration details

ENSAR2: European Nuclear Science and Applications Research - 2 <http://www.ensarfp7.eu>, UiO, ISOLDE, other contributors to the experiment?

Trond Wiggo Johansen

September, 2019



Contents

| | | |
|-------------------|---|-----------|
| 1 | Introduction | 11 |
| 2 | Theory | 13 |
| 2.1 | Oppgaveteksten (skal fjernes!) | 17 |
| 3 | Coulomb excitation experiment | 21 |
| 3.1 | ISOLDE at CERN | 21 |
| 3.2 | Experimental setup | 22 |
| 3.2.1 | Beam production | 22 |
| 3.2.2 | Target | 25 |
| 3.2.3 | Miniball spectrometer | 25 |
| 3.3 | Data acquisition system | 27 |
| 4 | Data analysis | 33 |
| 4.1 | Data handling | 33 |
| 4.1.1 | Counting and naming convention | 35 |
| 4.2 | Data conversion | 35 |
| 4.3 | Detector calibration | 36 |
| 4.3.1 | Simulation | 38 |
| 4.3.2 | Online calibration of particle detector | 39 |
| 4.3.3 | User calibration of particle detector | 41 |
| 4.3.4 | Threshold | 46 |
| 4.3.5 | Time calibration | 49 |
| 4.3.6 | Gamma | 51 |
| 4.3.7 | Doppler correction | 53 |
| 4.4 | Data analysis | 53 |
| 5 | Experimental results | 59 |
| 6 | Discussion | 61 |
| 7 | Summary and outlook | 63 |
| Appendices | | 65 |
| Appendix A | Symbol list | 67 |
| Appendix B | Acronyms and abbreviations | 69 |
| Appendix C | Computer setup and environment | 71 |
| C.1 | The computer | 71 |

| | | |
|---------------------|--|-----------|
| C.2 | The environment | 71 |
| C.3 | Run time | 72 |
| Appendix D | Two-particle collision | 73 |
| D.1 | Laboratory (LAB) frame of reference | 73 |
| D.2 | Center of mass (CM) frame of reference | 76 |
| D.3 | Connection between the LAB frame and the CM frame | 78 |
| Appendix E | Connecting MiniballCoulexSort with ROOT | 83 |
| Appendix F | Running ROOT and MiniballCoulexSort from anywhere in the terminal | 85 |
| Appendix G | CD simulation | 87 |
| Bibliography | | 91 |

Chapter 1

Introduction

+ Motivation

The experiment has been done before, with lower energy (and another target), Malin Klintefjord. <http://urn.nb.no/URN:NBN:no-56121>

Malin Klintefjord PhD thesis [1] with the three papers [2], [3] and [4] on ^{140}Sm .

Experiment conducted 8th - 14th of August 2017.

Expect to measure transition probabilities $B(E2)$ and quadrupole moment (nuclear deformation).

Tilbakemelding:

old REX-ISOLDE post-accelerator limited to 2.8 MeV/u (low Coulomb excitation cross section, low probability for multi-step excitation). Mo target was chosen to maximize cross section at this energy, and to normalize $B(E2; 0^+ \rightarrow 2^+)$ value in ^{140}Sm to the well-known $B(E2)$ value for the target.

New HIE-ISOLDE: energies up to 10 MeV/u \implies we can choose high-Z target (Pb) \implies high Coulex cross section, especially for multi-step. Also: $B(E2)$ for ^{140}Sm now known from previous experiment (and a lifetime measurement) \implies no need for normalization: we can use the known $B(E2; 0^+ \rightarrow 2^+)$ to normalize the transition probabilities for the higher-lying transitions. Chosen 4.7 MeV/u as the highest possible energy that is safe for Pb (distance of closest approach large enough to exclude nuclear interaction.)

All of my scripts are available in my GitHub repository found at <https://github.com/wiggoen/MasterThesis>.

Chapter 2

Theory

table of nuclides (HFB-style): http://www-phynu.cea.fr/science_en_ligne/carte_potentiels_microscopiques/carte_potentiel_nucleaire_eng.htm

$\beta - \gamma$ triangle: http://www-phynu.cea.fr/science_en_ligne/carte_potentiels_microscopiques/noyaux/zz62/zz62nn78all_eng.html

Table 2.1: Values of the fundamental physical constants from the National Institute of Standards and Technology (NIST) Physics Laboratory [5].

| Quantity | Symbol | Numerical value | Unit |
|--------------------------|--------|------------------------------------|------|
| Speed of light in vacuum | c | 299792458 | m/s |
| Elementary charge | e | $1.602176634 \cdot 10^{-19}$ | C |
| Electron volt | eV | $1.602176634 \cdot 10^{-19}$ | J |
| Atomic mass unit | u | $1.66053906660(50) \cdot 10^{-27}$ | kg |

Isotope notation:

$${}^A_Z X_N^Q$$

where X is the chemical symbol of the element, A is the nucleon number (mass number, $A = Z + N$), Z is the atomic number (proton number), N is the neutron number and Q is the charge ($Q = Z$ protons – i electrons).

Why CoulEx? https://iks32.fys.kuleuven.be/wiki/brix/images/5/58/10_20151123_Illana_BriX15_web.pdf

Magic numbers: 2, 8, 20, 28, 50, 82, 126

Maria Goeppert Mayer “discovered” them in ~1945. Observation of periodicity in binding energy \Rightarrow shell model for nuclei.

Eugene Wigner believed in liquid-drop model, did not trust new theory \Rightarrow called these numbers “magic”.

Source: https://ocw.mit.edu/courses/nuclear-engineering/22-02-introduction-to-applied-nuclear-lecture-notes/MIT22_02S12_lec01.pdf

Quadrupole deformation of nuclei.

Shape coexistence possible for certain regions of N and Z .

- triaxial shape / shape coexistence
- benchmark for theoretical models
- transition probabilities and quadrupole moments between several excited states are not known
- fundamental research

COULEX:

- nucleus excited by electromagnetic interaction.
- de-excitation \rightarrow gamma

Tilbakemelding:

shape coexistence often found near closed shells. Example: neutron deficient Hg nuclei ($Z = 80$ just below 82 shell closure, $N \sim 104$: neutron mid-shell).

^{140}Sm : $N = 78$, just below $N = 82$ shell closure, $Z = 62$: mid-shell.

Typical indication for shape coexistence: 0^+ states (often at low energy).

^{140}Sm was thought to have a low-lying 0^+ state [Firestone], but this state was shown to be 2^+ [Suoranczyk?]. Indication for 0^+ states around 1.5 MeV.

One of the objectives of this experiment: clarify the nature/structure of these 0^+ states.

Shape transition: Sm-144 ($Z = 62$, $N = 82$) spherical. Adding neutrons: transition of $N = 90$ from spherical to prolate deformed \rightarrow shape-phase transition, so called X(5) critical-point symmetry.

Taking out neutrons: very neutron-deficient Sm nuclei are also prolate deformed (e.g. Sm-132), but for ^{140}Sm : indication for triaxiality/ γ -softness [Klintefjord] \rightarrow another form of shape-phase transition/critical point behavior \implies E(5) [Iachello?]. ^{140}Sm could be one of the best examples for E(5) symmetry \implies need transition probabilities from higher-lying states to confirm.

Some suggestions:

- general things about nuclei shapes
- multipole expansion, shape parameters (5 parameters, 3 for space, 2 for deformation β, γ), ...
- quadrupole moments: intrinsic (body-fixed frame), spectroscopic (lab frame)
- transition probabilities, el.magn. matrix elements
- rotations and vibrations \rightarrow energy spectra, $B(E2)$ values

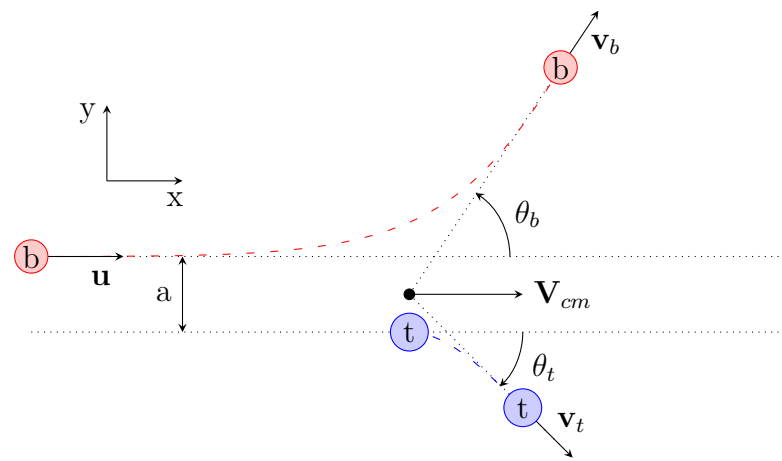
- Casten triangle (spherical vibrator, deformed rotor, γ -soft + X(5), E(5)), expected spectrum for E(5) nuclei

- the basics of Coulomb excitation

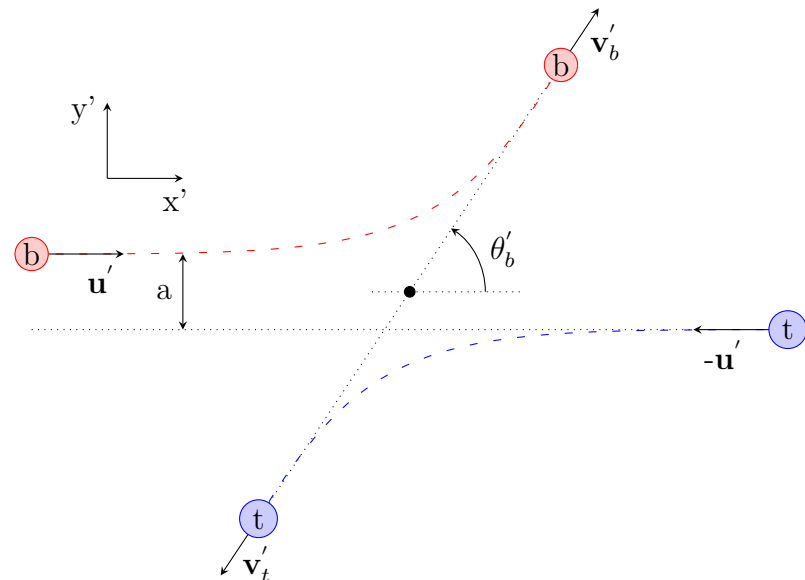
LISE++ [6]

Table 2.2: LAB vs. CM. Based on LAB input angles from θ_b and θ_t . From LISE++ kinematics calculator (reaction from the middle of the target).

| (a) $\theta_b \in [22.0^\circ, 56.7^\circ]$. | | | (b) $\theta_t \in [22.0^\circ, 56.7^\circ]$. | | |
|---|----------------|-----------------|---|----------------|-----------------|
| LAB | CM | | LAB | CM | |
| θ_b [°] | θ_t [°] | θ'_b [°] | θ_b [°] | θ_t [°] | θ'_b [°] |
| 22.0 | 71.7 | 36.6 | 40.6 | 56.7 | 66.6 |
| 26.0 | 68.4 | 43.2 | 42.3 | 55.3 | 69.4 |
| 29.1 | 65.9 | 48.2 | 44.2 | 53.9 | 72.2 |
| 32.2 | 63.4 | 53.3 | 46.1 | 52.4 | 75.2 |
| 35.2 | 60.9 | 58.1 | 48.3 | 50.7 | 78.6 |
| 37.9 | 58.8 | 62.4 | 50.6 | 49.0 | 82.0 |
| 40.4 | 56.8 | 66.3 | 53.1 | 47.1 | 85.8 |
| 42.8 | 54.9 | 70.1 | 56.0 | 45.0 | 90.0 |
| 45.0 | 53.2 | 73.5 | 59.1 | 42.8 | 94.4 |
| 47.1 | 51.6 | 76.7 | 62.5 | 40.4 | 99.2 |
| 49.0 | 50.2 | 79.6 | 66.1 | 37.9 | 104.2 |
| 50.7 | 48.9 | 82.1 | 70.2 | 35.2 | 109.6 |
| 52.4 | 47.6 | 84.7 | 75.0 | 32.2 | 115.6 |
| 53.9 | 46.5 | 86.9 | 80.2 | 29.1 | 121.8 |
| 55.3 | 45.5 | 88.9 | 85.8 | 26.0 | 128.0 |
| 56.7 | 44.5 | 91.0 | 93.8 | 22.0 | 136.0 |



(a) Scattering in the laboratory (LAB) frame. A small angle θ_b means forward scattering of the beam, a larger distance between the beam particle and the target particle, a weaker electromagnetic (EM) field and less excitation probability. A large angle θ_b means backward scattering of the beam, a closer distance between the beam particle and the target particle, a stronger EM field and a higher excitation probability.



(b) Center of mass (CM) frame.

Figure 2.1: LAB vs. CM frame.

NOTES TO BE REMOVED!!

2.1 Oppgaveteksten (skal fjernes!)

Oppgavens mål:

The ISOLDE facility at CERN has been upgraded to provide higher energies and intensities for radioactive ion beams. A new experiment to study ^{140}Sm was performed in the summer of 2017. The goal of the experiment was to measure electromagnetic transition probabilities and electric quadrupole moments for several excited states in ^{140}Sm by measuring Coulomb excitation probabilities. A large data set was obtained using silicon detectors to determine the energies and angles of scattered particles, and germanium detectors to measure gamma rays from excited states in ^{140}Sm .

The goal of the master thesis is to analyze the data from this experiment. The required tasks include development and improvement of data analysis software to determine Coulomb excitation yields. These yields will then, in a second step, be compared to theoretical calculations and transition probabilities and quadrupole moments will be extracted using chi-square minimization procedures.

Prosjektbeskrivelse (omfang 60 studiepoeng):

The shape of an atomic nucleus is determined by a delicate interplay between macroscopic (liquid drop) properties and microscopic shell effects. Nuclei with filled proton or neutron shells (i.e. magic nuclei) are generally spherical in shape, whereas nuclei with open shells gain energy by assuming a deformed shape. Depending on the occupation of specific orbitals, the nuclear shape can change drastically by adding or removing protons or neutrons. Certain nuclei exhibit shape coexistence, i.e. the coexistence of quantum states that correspond to different shapes. Because the shape of a nucleus is so sensitive to the underlying nuclear structure and to changes of the proton and neutron numbers, the excitation energy, or the angular momentum, observables related to the nuclear shape are used as benchmarks for theoretical models.

Nuclei in the rare earth region, and in particular the chain of samarium isotopes, exhibit a variety of shape effects. The Sm isotope with closed neutron

shell at N=82, ^{144}Sm , is spherical in shape. Adding neutrons to ^{144}Sm changes the deformation to an elongated (prolate) quadrupole shape. The transition from spherical to prolate shape, which occurs for ^{152}Sm at N=90, can be interpreted as a shape-phase transition. Flattened (oblate) quadrupole shapes are predicted by theory to occur below the N=82 shell closure. An earlier experiment studying ^{140}Sm at CERN-ISOLDE found triaxial shape for this isotope, i.e. a shape where all three principal axes of the ellipsoid have different lengths. ^{140}Sm can therefore be considered to lie at the critical point of a phase transition from spherical to deformed, and from prolate to oblate shape.

Foreløpig tittel:
Coulomb excitation of ^{140}Sm

Metoder som tenkes benyttet:
Multi-step Coulomb excitation with radioactive beam, isotope separation on-line technique, nuclear spectroscopy, particle-gamma and particle gamma-gamma coincidence analysis, advanced chi-square minimization procedures.

Sjekk sensorveiledning!!

Fjern blå linker in-text før innlevering!!

Experimental setup - other info sources

- ISOL & Post acceleration: https://www.euroschoolonexoticbeams.be/site/files/nlp/LNP700_contrib2.pdf
- ISOL RIB (2004): <http://accelconf.web.cern.ch/AccelConf/e04/PAPERS/TUXCH01.PDF>
- RIB (2017): <http://iopscience.iop.org/article/10.1088/1361-6471/aa990f/pdf>
- RIB: http://publications.lib.chalmers.se/records/fulltext/175494/local_175494.pdf
- RIB: <https://www.sciencedirect.com/science/article/pii/S0168583X02018864>
- Post-accelerated beams ISOLDE: <http://iopscience.iop.org/article/10.1088/1361-6471/aa78ca>

- PSB: <https://www.sciencedirect.com/science/article/pii/0168583X92959079>
- PSB: <https://home.cern/science/accelerators/proton-synchrotron-booster>
- RILIS ISOLDE: <https://www.sciencedirect.com/science/article/pii/S0168583X13008914>
- HIE-ISOLDE publications: <http://hie-isolde-project.web.cern.ch/hie-isolde-publications>
- Miniball pictures: <https://cds.cern.ch/record/844871?ln=en>
- The MINIBALL array [7]

DAQ:

- MAR_aBQU web page: <https://www-old.mll-muenchen.de/marabou/htmldoc/>
- MAR_aBQU file formatting: <https://www-old.mll-muenchen.de/marabou/htmldoc/marabou/IOSpec.html>

Chapter 3

Coulomb excitation experiment

3.1 ISOLDE at CERN

The acronym ISOLDE stands for Isotope Separator On Line DEvice. ISOLDE is a Radioactive Ion Beam (RIB) facility at CERN in Meyrin, Switzerland. [Figure 3.1](#) shows the CERN accelerator complex, where ISOLDE is located beside the Proton Synchrotron Booster (PSB). The facility can produce over 1000 different radionuclides to be used in a wide variety of experiments in nuclear physics, atomic physics, solid state physics, life sciences and fundamental interactions. Experiments have been performed at ISOLDE since 1967 and since 2001 experiments with post-accelerated RIBs have been conducted. The High Intensity and Energy upgrade (HIE-ISOLDE) have made it possible to deliver energies up to 10 MeV/ u in 2018 [8–10].

Most of the around 4000 characterized nuclides are radioactive [11]. In many cases it is not possible to make radioactive nuclei targets and perform an experiment because of the short half-life of the nucleus of interest. To study these radioactive nuclei, RIBs are used on stable targets. One way of obtaining a RIB is to use the Isotope Separator On Line (ISOL) method. In the ISOL method, two accelerator systems is needed. The first accelerator is used to produce the radioactive atoms at rest, and the second accelerator is used to accelerate these atoms [12].

In RIB facilities the energy and intensity is generally lower compared to stable beam facilities. This makes it suitable for Coulomb excitation and particle transfer reactions. The beam is the isotope of interest and since it is traveling with a significant velocity (v/c values of a few percent), the emitted γ -rays from de-excitation may have large Doppler shifts. Since the detectors have a finite solid angle, it can lead to a sizable Doppler broadening. When the detection system has high granularity, the Doppler shifts and broadening can be corrected for. If the angle between the recoiling nucleus and the γ -ray can be determined accurately, Doppler correction can be applied [13].

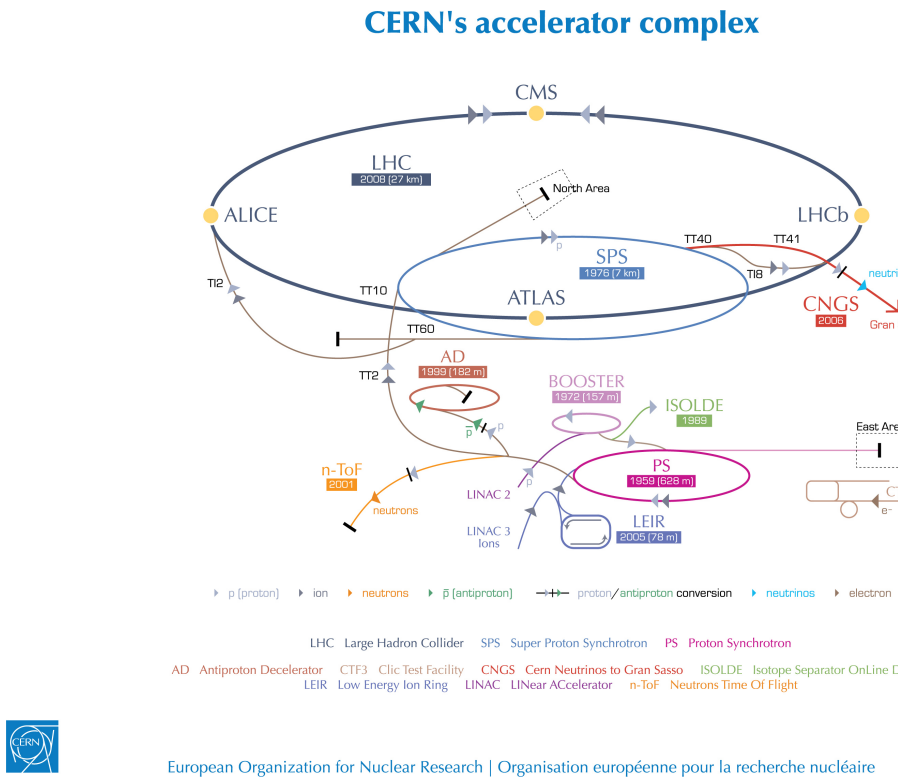


Figure 3.1: The CERN accelerator complex [14]. ISOLDE gets accelerated protons from LINAC 2 and the PS Booster.

3.2 Experimental setup

3.2.1 Beam production

Figure 3.2 shows a sketch of the experimental setup used in the ^{140}Sm Coulomb excitation experiment. A continuous flow of accelerated proton beam bunches from the PSB comes into the ISOLDE facility and collide with a thick production target. The proton beam has an energy of 1.4 GeV and an intensity up to $2 \mu\text{A}$. Two proton beam bunches are separated by 1.2 s [15, 16]. ISOLDE typically takes 50% [13] of all proton bunches from the PSB, the rest goes to the Large Hadron Collider (LHC) and other experiments shown in Figure 3.1. In the reaction between the proton beam and the production target, radioactive nuclides are produced in spallation, fission or fragmentation reactions (basically smashing the target into pieces) [9]. The production target is chosen from a stable region heavier than the nucleus of interest. In our experiment, a production target of tantalum (Ta, $Z = 73$) was used, producing the elements in the chart of nuclides up to Ta. A large amount of different isotopes is produced in this way, and the challenge is to extract the nucleus of interest. To obtain the nucleus of interest, we first have to use a method of selecting the atom of interest, and then the

nucleus of interest.

To get the atomic element of interest, one idea is to use a method of selective ionization and then a high voltage electrostatic field to extract the ions. Electronic transitions are characteristic for each chemical element. A laser with precisely tuned wavelength can obtain the photon energy that matches the electronic transition energies in the atom [17, 18]. Thus we can use one laser to excite an electron to a specific excited electron-state in the atom, a second laser to excite electrons further to another excited electron-state and a third laser to kick out the electron. In this way we only ionize the atomic element of interest. There could be contaminants from surface ionization (atoms that collide with the walls of the ion source), but this is detectable. Using periods of laser on and off, we can detect the resulting contaminants in the beam. The Resonance Ionization Laser Ion Source (RILIS) is based on the method of step-wise (2-3 step) excitation and ionization of the atom. It is an element-selective process which is used to produce ion beams of the correct element [19]. In this experiment RILIS was used to select samarium (Sm) with atomic number $Z = 62$.

At this point we have a continuous beam of Sm ions of 60 keV energy (the target is on a 60 kV high voltage platform) [9, 15]. The next step in the process is to have mass separation, and we need to give the continuous beam a fine structure, because the post-accelerator cannot accept a continuous beam coming in, it accelerates bunches. The beam can collide in one of two target stations, either the General Purpose Separator (GPS) or the High Resolution Separator (HRS). The GPS has one bending magnet and can deliver beams of different masses ($\pm 13\%$ of the central beam line mass) simultaneously into three beam lines, while the HRS has two bending magnets with high mass resolving power which delivers the beam into the main (central) beam line [15, 20]. In this experiment the GPS was used to select the isotope of Sm with mass number $A = 140$.

Now we have a continuous beam of ^{140}Sm . The mass separator also gets rid of contaminants that come out of RILIS but have different mass. There could still be isobaric contaminants from surface ionization but luckily there is very little surface ionization for the neighboring elements of Sm. In the Radioactive beam EXperiment TRAP (REXTRAP) we collect the ^{140}Sm ions, so that we can release them in bunches that are matched to the fine structure of the LINear ACcelerator (LINAC). REXTRAP is a penning trap which has the tasks of accumulation, bunching and cooling of the RIB [8, 21, 22]. The ions are released in bunches and transferred to the REX Electron Beam Ion Source (REXEBS).

REXEBS is a charge breeder where the RIB is bred to a high charge state [23], with a mass-to-charge (A/q) ratio typically between 2.5 and 4.5 [24]. REXEBS releases the beam with a certain energy through a mass separator and into the HIE-ISOLDE LINAC [8]. To accelerate the charged ions (the beam) to high energy, we need highly charged ions. The EBIS blasts off more electrons from

Sm, which leaves the nucleus in a high charge state, going from $^{140}\text{Sm}^{+1}$ to $^{140}\text{Sm}^{+34}$ ($A/q \approx 4.1$). The longer the ions stay in REXEBIS, the higher the charge state becomes. We get a distribution of charge states, and we loose those that have the wrong charge state because the LINAC can only accept one charge state [25–28].

The HIE-ISOLDE LINAC accelerates the beam of ^{140}Sm ($T_{1/2} = 14.82$ min) with excellent purity to 4.65 MeV/u (total energy 651 MeV) through the beam line, and magnets bend the beam into the Miniball spectrometer, where the particles and γ -rays are detected. This experiment was one of the first Miniball experiments with the new upgraded superconducting accelerator.

To have a successful experiment, the purity of the beam is of great importance. Contaminants in the beam can come from different sources [13]. From the primary target we can have:

- isobaric contaminants which are inseparable by the mass separator because of the same mass number
- isotopes with an integer multiple of both mass and charge

and from stable isotopes the contaminants can come from:

- buffer gas in REXTRAP (e.g. Ne, Ar)
- residual gas in REXEBIS (e.g. C, O)
- components of REXEBIS (e.g. La from the cathode)

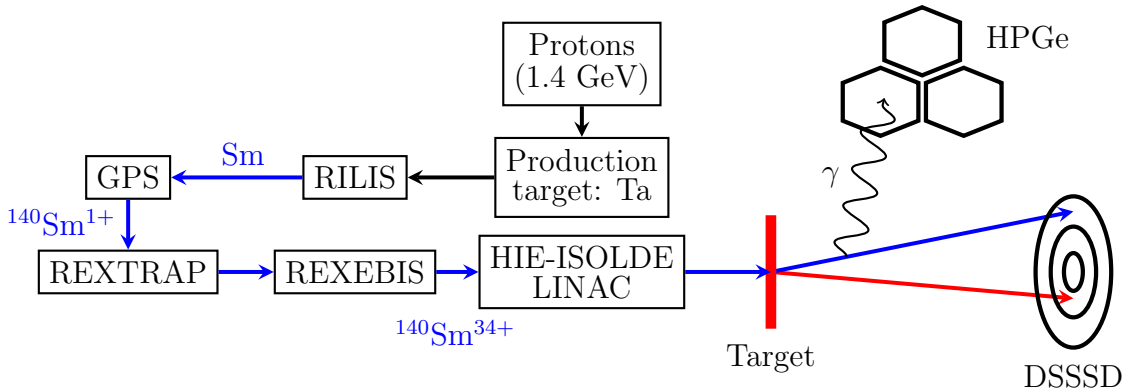


Figure 3.2: The Coulomb excitation setup at ISOLDE (experiment code: IS558, which was titled Shape Transition and Coexistence in Neutron-Deficient Rare Earth Isotopes). Adapted from [1].

3.2.2 Target

As a target, ^{208}Pb with a thickness of 1.4 mg/cm^2 was chosen. The reason for the choice is that it is very hard to excite ^{208}Pb since it's doubly magic. We wanted the highest possible Z ($= 82$) of a stable isotope to get maximum excitation probability.

Since we don't need normalization (because we have the $B(E2, 0_1^+ \rightarrow 2_1^+)$ from the previous experiment [4] and from lifetime measurement [29]), we have chosen a target that is very hard to excite, so transitions from the target will not complicate the spectrum.

^{208}Pb has no quadrupole deformation, the first excited state ($2615 \text{ keV}, T_{1/2} = 16.7 \text{ ps}$) is of octupole vibration ($J^\pi = 3^-$). If we are [lucky/unlucky?](#) we might see a little bit of this first excited state in the spectrum. This happens if the "collision" is almost head on, and the target hits one of the inner rings.

Unfortunately there was a finger print on the target, so even before beginning the experiment, we have some contamination (probably carbon).

3.2.3 Miniball spectrometer

[Figure 3.3](#) shows an overview picture of the Miniball spectrometer.

Target chamber

The target chamber is a hollow sphere made out of a machined out, single piece of aluminium alloy (AlMg_3), with a thin wall and an inner radius of approximately 80 mm. Inside the chamber we find a target wheel and a particle detector. The target wheel can hold up to six different targets as shown in [Figure 3.4](#). The particle detector can be positioned 25 - 31 mm from the target wheel, limited by the space inside the chamber. Outside of the target chamber the average distance from each γ -detector cluster to the center of the target chamber is approximately 10 cm. The forward detectors and the backward detectors has an angular position θ of approximately 45° and 135° respectively, compared to the beam line. In the vertical plane, perpendicular to the beam line, the four γ -detectors in forward and backward position are placed roughly on a circle with a separation of $\phi = 90^\circ$ [13].

Particle detector, DSSSD (CD)

To detect the scattered beam and target nuclei, a segmented Double Sided Silicon Strip Detector (DSSSD) composed of four quadrants was used. The DSSSD looks very like an audio Compact Disc (CD), and hence it is called the CD. In the front of the CD, one quadrant consists of 16 annular strips (rings) with a pitch of 2 mm, while the back consists of 24 sector (radial) strips with a pitch of 3.5° .

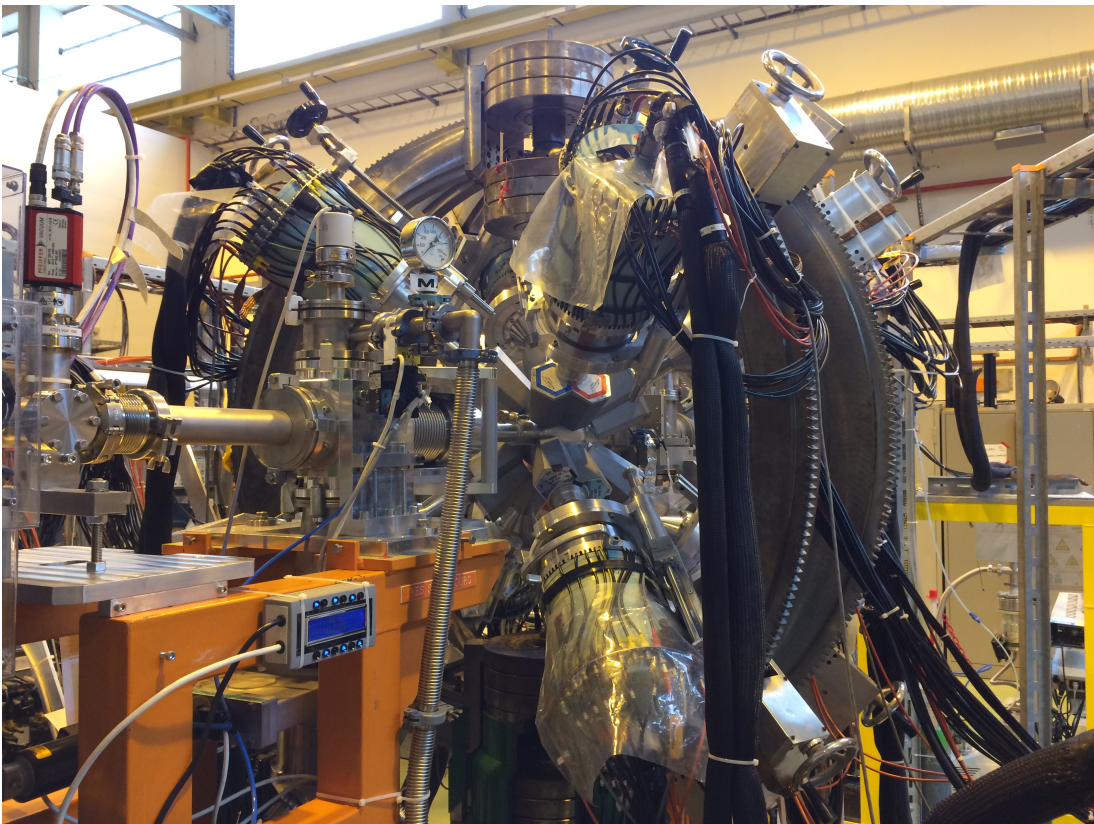


Figure 3.3: Overview picture of the Miniball spectrometer.

Photo by: Trond Wiggo Johansen.

The innermost strip has an inner radius of the active area of 9 mm, while the outermost strip has an outer radius of the active area of 40.9 mm. There are in total 160 discrete detector elements for all four quadrants (64 in front, 96 in back). Each quadrant is connected to its own Analog to Digital Converter (ADC). Because of lack of available channels in the ADC, the sector strips in the back are paired up, so that it is effectively 12 sector strips in the back side. The CD detector has a total area of 5000 mm^2 , where the active area is approximately 93%. The silicon wafer thickness is between $50 \mu\text{m}$ and $1000 \mu\text{m}$ with a dead layer of 0.3 to $0.8 \mu\text{m}$ of aluminium. For simplicity the dead layer thickness is usually assumed to be $0.7 \mu\text{m}$ [13, 30]. Table 3.1 shows some of the specifications of the CD and Figure 3.5 shows a sketch of the front and back side. The distance¹ from the target to the CD was 26.98 mm ($\pm 1 \text{ mm}$). In the laboratory (LAB)

¹The source has a thickness of 1.23 mm, which needs to be factored in so that the target to CD distance is the CD to source distance plus the source thickness, that is $25.78 \text{ mm} + 1.23 \text{ mm} = 27.01 \text{ mm}$. The source data was reanalyzed since this original log entry, giving a 0.03 mm difference. From private communications at ISOLDE in August 2018, the distance from the target to the CD was determined to be 26.98 mm.”

reference frame the CD has a angular coverage between 18.4° and 56.6° . An extensive description of the CD can be found in [31].

Table 3.1: CD specifications.

| | Annular strips (CD Front) | Secular strips (CD Back) |
|-----------------------------|------------------------------|-----------------------------|
| Number of strips | 16 | 24 |
| Inner radius of active area | 9.000 mm | - |
| Outer radius of active area | 40.900 mm | - |
| Strip pitch | 2.000 mm | 3.5° |
| Strip width | 1.900 mm | 3.4° |
| Strip length | - | 31.900 mm |
| Active angle coverage | 81.6° | - |
| Inner strip distance | - | 0.100 mm |

γ detectors, high-purity germanium (HPGe)

In Coulomb excitation experiments the target chamber is surrounded by the γ detectors as shown in Figure 3.6. The γ -ray spectrometer consists of a total of 24 six-fold segmented High-Purity Germanium (HPGe) crystals, which are divided into 8 clusters of 3 crystals each. Each crystal is encapsulated and segmented into 6 parts, making a total of 144 segments. For maximum efficiency, the detectors are placed in a compact geometry around the target chamber [13, 32]. The detector-array can cover a solid angle of about 60% of 4π , when the optimum distance between the target chamber and the HPGe-clusters is achieved. The average energy resolution at $E_\gamma = 1.3$ MeV is 2.3 keV [33]. From each detector we get seven signals in total for each event, one from the core and six from each segment. This requires 168 channels for data aquisition. The shapes of these signals is analyzed to get information of the position. Because of the segmentation of the detector, a better Doppler correction can be performed compared to using the whole crystal. During operation the HPGe-clusters needs to be cooled down by liquid nitrogen and there is an automated filling system in place for this [32].

3.3 Data acquisition system

Signals from the CD and the HPGe clusters are read out by the ADC and Digital Gamma Finder (DGF) modules and sent to a Personal Computer (PC) in the Data AcQuisition (DAQ) room at ISOLDE where the data is then stored. The collection of data is done by the MAR_aBQU [34] DAQ system [13]. It is split in two parts as shown in Figure 3.7, one front-end part based on the Multi Branch System (MBS) [35] and one back-end part based on the ROOT framework [36].

The front-end takes care of data readout, event building and data transportation, while the back-end takes care of the setup, run control, histogramming, data analysis and data storage. The system can manage high counting rates without dead time, where the limitation is essentially only pile-up. The ADCs and TDCs can buffer up to 32 events at a time [13].

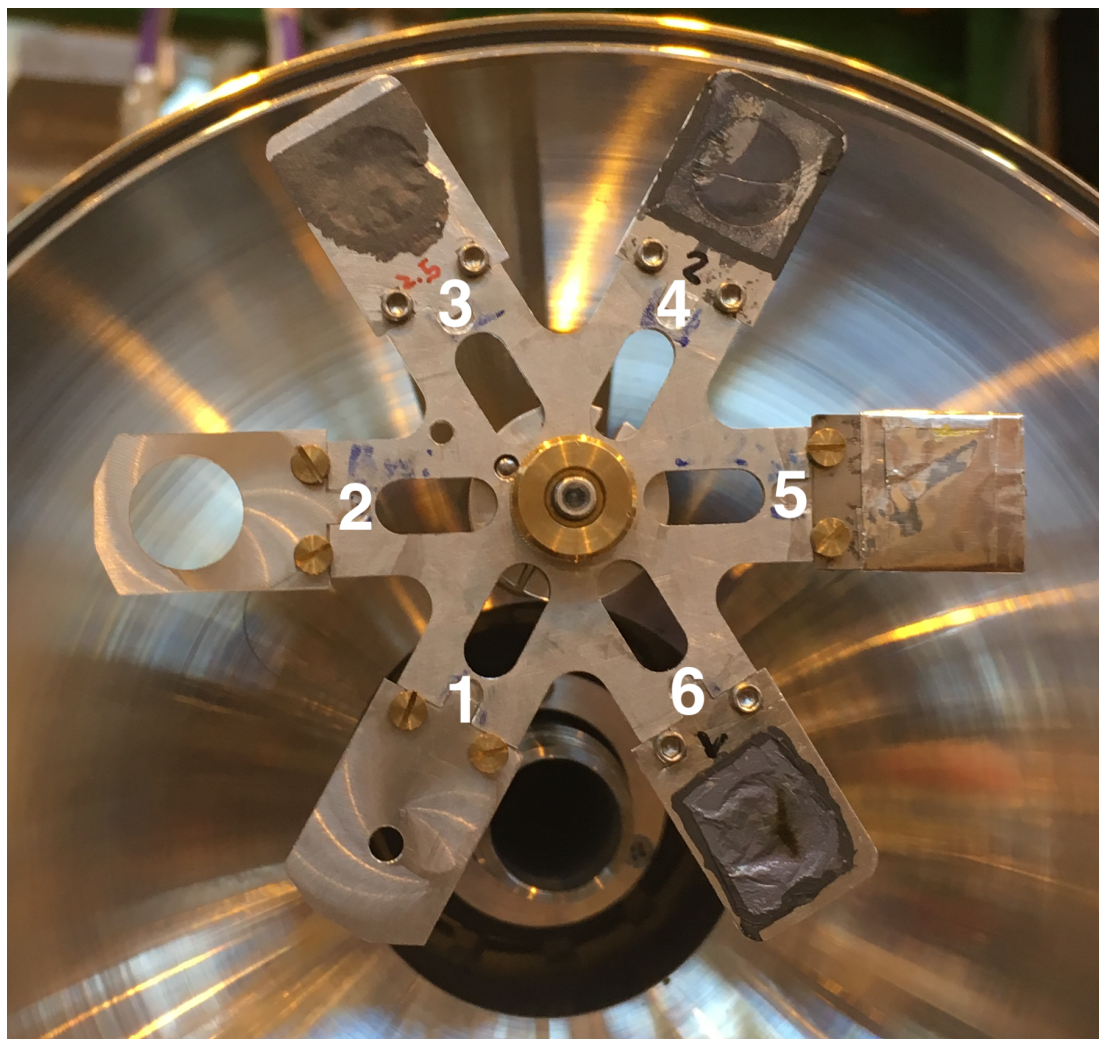
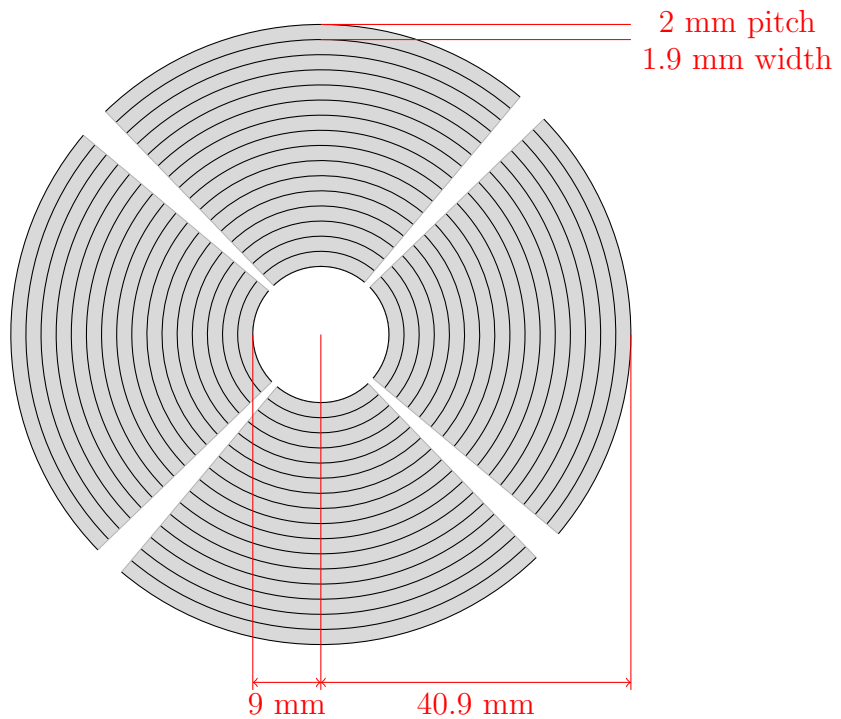
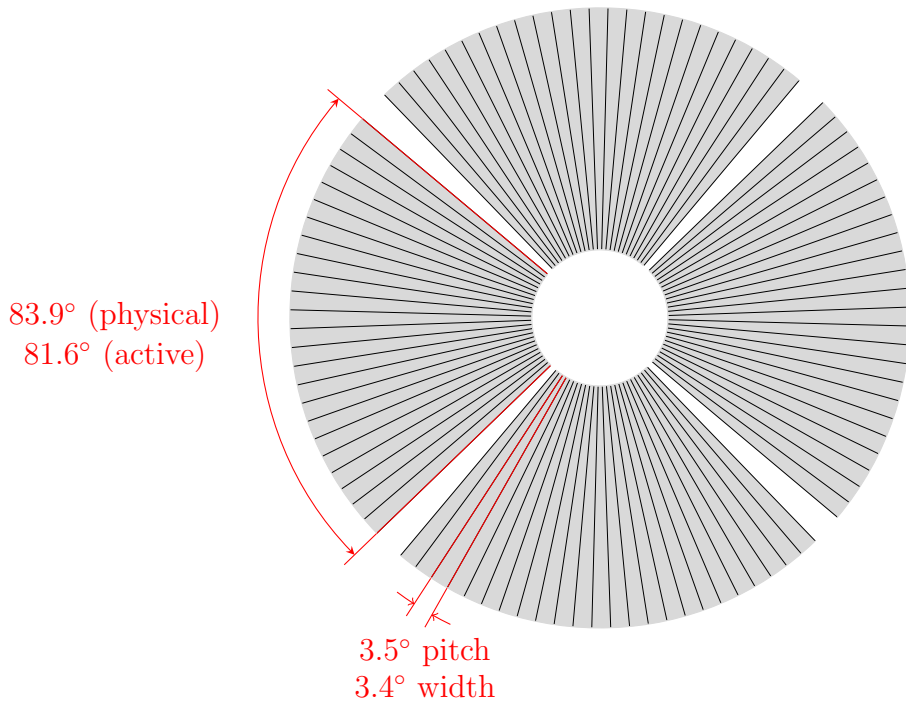


Figure 3.4: The target wheel can hold up to six different targets. Position 6 has the target ^{208}Pb with thickness 1.4 mg/cm^2 .

Photo by: Liam Gaffney, date: 07.08.2017.



(a) CD front: The numbering of the strips goes from strip 0 (outermost) to strip 15 (innermost). Quadrants are numbered in clockwise direction with respect to the beam direction, so that left is 1, up is 2, right is 3 and down is 4.



(b) CD back: The numbering of the strips goes from strip 0 to strip 23 in counter-clockwise direction viewed from this side. Quadrants are numbered in clockwise direction with respect to the beam direction. From this perspective right is 1, up is 2, left is 3 and down is 4.

Figure 3.5: CD sketch, adapted from [30].

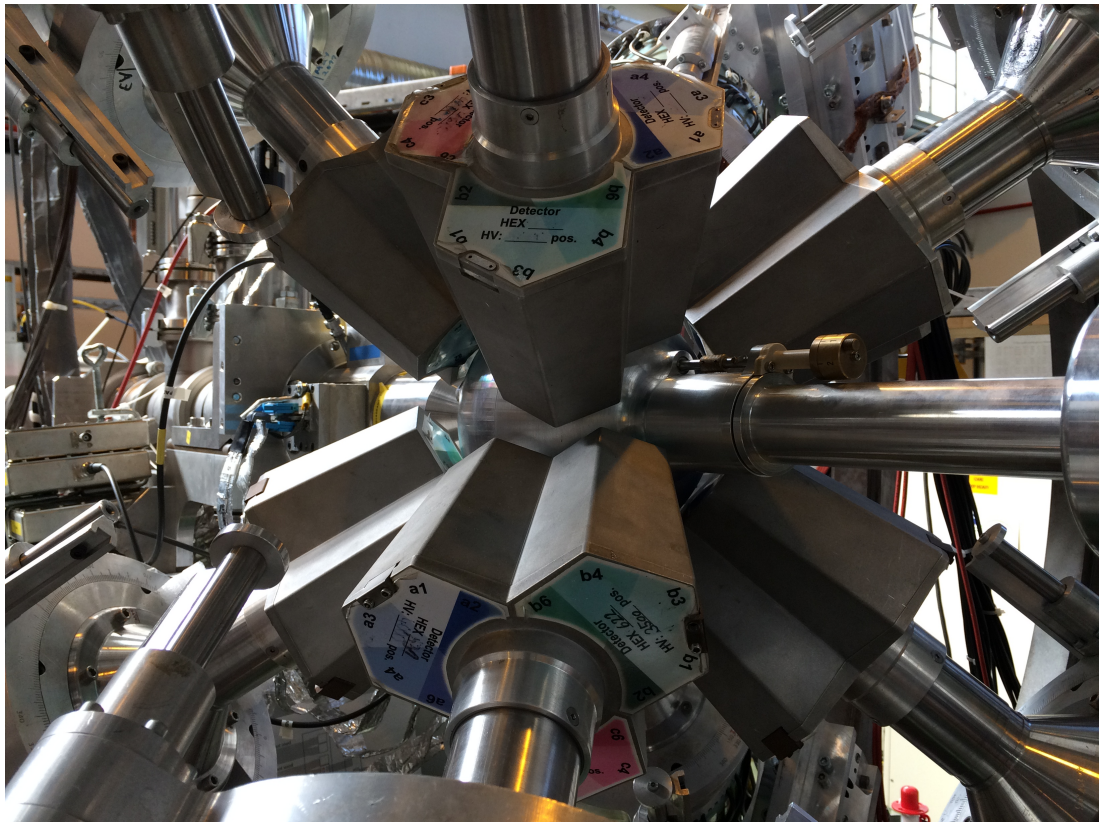


Figure 3.6: Close up picture of the Miniball spectrometer. The Miniball target chamber is in the middle, surrounded by the triple-cluster encapsulated γ crystals. The beam line goes through the target chamber.

Photo by: Trond Wiggo Johansen.

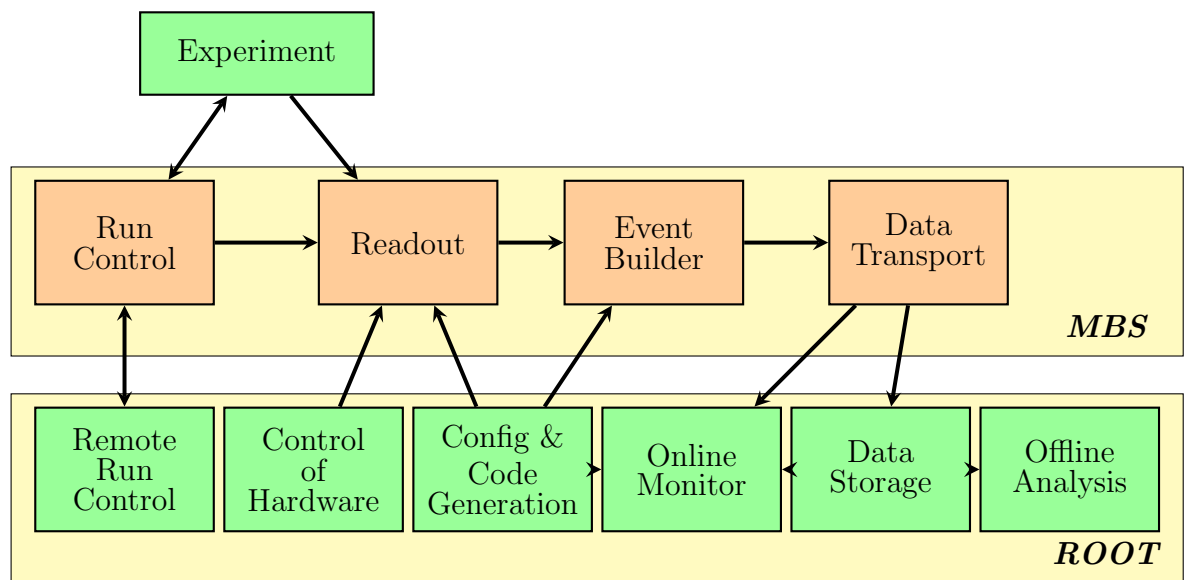


Figure 3.7: MARaBQU tasks, adapted from [34].

Chapter 4

Data analysis

4.1 Data handling

The raw data from Miniball experiments essentially¹ comes in list mode (identification, energy, time), where every line is an event. It is stored in **.med**-files (MBS Event Data, or also known as Miniball Event Data) with the naming convention *140Sm_208Pb_pos6_0xy.med*, where *x* and *y* are numbers between 0 and 9. The goal of the data is to obtain Doppler-corrected γ -spectra with various conditions on particles and angles, in order to analyse the Coulomb excitation of ^{140}Sm .

```
$ cd ~/GitHub/MasterThesis/Raw_data/Sm
$ root 140Sm_208Pb_pos6_008_OnBeam.root
root [1] tr->Show(10)
===== EVENT:10
Event          = (BuiltEvent*)0x7f8db0469010
fUniqueId      = 0
fBits          = 33554432
ebisTime       = 16936792
t1Time         = 0
superCycleTime = 65948
eventNumber    = 100
subEventNumber = 12
dggfData       = (vector<DggfData*>)0x7f8db04690c0
dggfData.fUniqueId = 0
dggfData.fBits   = 33554432
dggfData.fModuleNumber = 18
dggfData.fChannel = 0
dggfData.fMultiplicity = 1
dggfData.fEventTime = 40774
dggfData.fEnergy = 583
dggfData.fFastTriggerTime = 40799
dggfData.fLongFastTriggerTime = 16949087
```

¹The format is not entirely correct, since it has identification of where the particle and γ hit. A more detailed format could be: time, cluster, crystal, sector, ring/strip, energy, etc.

```
dgfData.fUserValues[6] = 26112 , 60811 , 32766 , 0 , 38240 ,
60811
```

A sorting and analysis code named *MiniballCoulexSort* [37] written in C/C++ is the preferred code to use for Miniball experiment data. It is under constant development at CERN-ISOLDE under the management of Dr. Liam Gaffney². The main steps of how to download, install³ and use it is outlined in the `README.md` file in the GitHub repository for Miniball, linked in the reference. Unfortunately the code isn't very well documented, so it takes some time to learn what it does and how to use it. To get from the raw data to the Doppler-corrected γ -spectra, the code is broken down in a three step procedure:

1. `MedToRoot`

- converts the raw data to ROOT format

2. `TreeBuilder`

- event building
 - calibrate detectors and apply thresholds
 - use particle- γ coincidences (correlations) to build events
 - store everything in a tree structure for easy access

3. `CLXAna`

- apply gates on particles and perform Doppler correction

One program that is mentioned in the Miniball GitHub repository, but not showed how to use, is the `AQ4Sort`. It is used in the same way as the `TreeBuilder` script, but it sorts the histograms in another way and it does not take any command line flag options. This program is used before and during the calibration of the particle detectors, because it gives information about every single ring and every single back strip (the pixels of the CD).

`TreeBuilder` takes a number of flag options. If the `-cdpad` flag option is not used, then there will be no particle events, because they come in the CD. The `-s` flag (singles) is for adding particles which come without a γ -ray and the `-addback` flag is for adding Compton scattered events together in the Miniball clusters.

²Dr. Liam Gaffney is a research fellow at ISOLDE, affiliated with Miniball.

³If the `make` step fails, try doing a `make clean` and then `make`. The code might think that it is already built.

4.1.1 Counting and naming convention

In the following sections I will introduce different programs and scripts used in the data calibration and analysis. One thing to note here, is that the numbering of the CD rings and strips are different in these programs and scripts.

Histograms sorted by `TreeBuilder` starts counting from 0 (outermost ring) to 15 (innermost ring) with energy in MeV showed in [Figure 3.5](#). In `AQ4Sort` it starts from 1 (innermost ring) to 16 (outermost ring) with energy in keV. [Table 4.1](#) shows the ADC wiring and a comparison of the histogram naming from `TreeBuilder` and `AQ4Sort` can be found in [Table 4.2](#). The simulation program `kinsim3` counts from 1 (innermost ring) to 16 (outermost ring), the opposite of `AQ4Sort`. It is easy to be confused by all the different counting, but I will try to use the counting order of `kinsim3` for everything, it seems like the most logic way of counting. I cannot change the wiring of the CD, but I can choose the most logic order of counting for me.

4.2 Data conversion

In order to analyze the data in the ROOT⁴ framework, the first part of the code is just to convert the `.med`-files produced by MAR_aBQJU into `.root`-files with the program `MedToRoot`. In order to not copy and paste the commands used with `MedToRoot` in the terminal for every data file, I made a bash script called `M2R.sh` to do this. It uses `MedToRoot` to take in as many files as you want, and convert it in one go. It takes one command line argument because it was initially developed to sort different elements, so it is fairly simple to expand. By not using any command line arguments, the script will print out how to use it. First all of the interesting files are converted with the `M2R.sh` script. An example of the use with terminal output for the `.med`-file with $xy = 08$ is as follows:

```
$ cd ~/GitHub/MasterThesis/Scripts/sorting
$ ./M2R.sh Sm
opening file ../../Raw_data/Sm/140Sm_208Pb_pos6_008.med ...
EventBuffer :: EventBuffer( GlobalSettings *)
Processing event number      0
Start trigger #14

Processing event number 130000
Stop trigger #15

Unpacked 132802 events:
wrong dgf hit pattern:          0 ( 0.0 %)
wrong adc headers:             0 ( 0.0 %)
```

⁴ROOT is a data analysis framework written in C/C++ made at CERN.

```

# of overflows in adc channels:      599712 (451.6 %)
# of underflows in adc channels:    0 ( 0.0 %)
pattern unit mismatches:          0 ( 0.0 %)

Number of ebis pulses:           66351
Number of t1 pulses:             2211
Number of supercycle pulses:     429
committed           1 243 951 987 bytes to tree tr, 'Tree for on
beam data of Coulex setup@Miniball'
and                 15 338 250 bytes to tree bg, 'Tree for on
beam background data of Coulex setup@Miniball'
and                 237 454 436 bytes to tree tr, 'Tree for off
beam data of Coulex setup@Miniball'
wrote                97 189 bytes to file ../../Raw_data/Sm
/140Sm_208Pb_pos6_008_OnBeam.root => compressed by a
factor of 12799.3
,                  18 362 bytes to file ../../Raw_data/Sm
/140Sm_208Pb_pos6_008_OnBeamBackground.root => compressed
by a factor of 835.3
,                  67 934 bytes to file ../../Raw_data/Sm
/140Sm_208Pb_pos6_008_OffBeam.root => compressed by a
factor of 3495.4
and                22 167 bytes to file ../../Raw_data/Sm
/140Sm_208Pb_pos6_008_Scaler.root => compressed by a
factor of 2769.1

```

For each file converted with `MedToRoot`, the program makes four files with the naming convention

- `140Sm_208Pb_pos6_0xy_OnBeam.root`
- `140Sm_208Pb_pos6_0xy_OnBeamBackground.root`
- `140Sm_208Pb_pos6_0xy_OffBeam.root`
- `140Sm_208Pb_pos6_0xy_Scaler.root`

where the file of interest is the first one. The `OnBeam.root`-files are the files used in the sorting and event building with `TreeBuilder` and/or `AQ4Sort`.

4.3 Detector calibration

Tilbakemelding:

start with explaining the general idea for the calibration:
determine centroids of peaks in spectra, compare with simulations (kinematics, energy loss) to get linear coefficients (gain + offset). You could show spectra for 2 rings: one where it is ok to get the 2 centroids for Sm and Pb, and one where it is difficult → use additional data (Ni?)

Sectors: cover wide angular range → no sharp peaks

Solution: gate on rings to see peaks in sectors and calibrate.

Idea:

1. produce spectra
2. set thresholds: example, explain criteria
3. find calibration coefficients → see above
explain strategy, show examples...
4. time calibration

if you try to write this step-by-step cook book, you could introduce your scripts wherever is the right place to use them.

The general idea of the calibration is to make sure that the energy spectra from the detectors have the same physical features, that the detectors show the same energy distribution at the same position for the same kind of particles or γ -rays hitting the same or the angular similarly place in the detector. We want to determine centroids of peaks in the spectra, compare these with simulations using kinematics of the reaction and energy loss, to get linear coefficients of the detectors.

Both detector types in this experiment are semiconductor detectors. Except for silicon (as the CD), semiconductors generally require cooling to low temperatures before they can be operated. The basic principle of operation is that incoming ionizing radiation⁵ creates electron-hole pairs in the semi-conducting material which are then collected by an electric field. The number of electron-hole pairs is proportional to the energy of the incoming radiation to the semiconductor [38].

Assuming a linear correlation between the energy E of the particle or γ -ray and the channel number n of the ADC, we get

$$E = g \cdot n + a \quad (4.1)$$

where a is the offset in keV and g is the gain in keV/ n . The offset a can be expressed easily from [Equation \(4.1\)](#) as

$$a = E - g \cdot n \quad (4.2)$$

To find the gain g , we need at least two measuring points, e.g. the peak energy of Sm and the peak energy of Pb for a given angle. The relationship can be written as

$$g = \frac{E_{\text{Sm}} - E_{\text{Pb}}}{n_{\text{Sm}} - n_{\text{Pb}}} \quad (4.3)$$

⁵For the CD, the ionizing radiation is the beam or target particles scattered from the reaction, while the ionizing radiation for the HPGe-detectors is the high-energy photons (γ) from de-excitation of the nuclei.

On the front side of the CD we only have two measuring points per angle interval⁶, while on the back side of the CD we have we have two peaks per secular strip that we can fit. By doing a Gaussian fit, we can get the centroids (channels of the peaks) for both Sm and Pb. For more than two centroids, we can use linear regression to find the best fit (this is the best option for the back side of the CD).

4.3.1 Simulation

To calibrate the data, we need to know the expected energy of the centroids of the peaks. This was done by simulating the experiment in a program called `kinsim3` [39]. The program is written in C++ by Dr. Liam Gaffney and the purpose of the program is to simulate the kinematics of an experiment. The simulations are theoretical predictions of the energy distribution of the peaks for each ring in the CD (it gives a simulated spectra for the CD and for every strip). These we fit, collect the centroid of and use in the calibration. The program uses SRIM-2013 [40] (the Stopping and Range of Ions in Matter) generated files relevant to the scattering/reaction? and it takes into account the energy loss in the dead layer of the detector, which is energy and angle dependent. The SRIM-files used in this simulation can be found in *MasterThesis/SRIM*. For the Si dead layer, the SRIM-files must have units of MeV/mm. (If you are using MeV/cm², you must change the distance on line 359 to be in the correct units. The correction factor is at the bottom of the SRIM file.)

`kinsim3` generates pdf-files of the stopping powers automatically. The rest of the plots are available inside the generated `.root`-file. To get the energy simulation for each ring, the function `simulation_plots()` from the script `ParticlePlot.cpp` was used.

Tilbakemelding:

what are the ingredients for this simulation?

simple 2-body kinematics: energy of projectile, scattering angle of projectile \Rightarrow energy of scattered projectile, {angle, energy} of binary partner (target recoil)
Stopping powers (which models?) \rightarrow SRIM

Slowing of the particles in the target and in the dead layer of Si

Terminal: Simulation: ^{140}Sm on ^{208}Pb :

```
$ cd ~/GitHub/Miniball/kinsim
$ root
root [0] .L kinsim3.cc+
root [1] kinsim3(62, 82, 140, 208, 1.4, 4.65, 0.02, 1.0, 0.6,
26.98, false, 1e6, "../SRIM")
```

⁶Not entirely true, since we have three peaks in the spectra. But since we don't know what the contaminant is, we effectively only have two known measuring points.

```
... <showing output from program>
root [2] .q
$ mv 140Sm_208Pb_1.4mg_4.65MeVu_d0.02MeVu_res0.6.root ../../
MasterThesis/Sorted_data/sim_140Sm_208Pb.root
```

After the simulation program was run, I moved and renamed the file with the **mv** command.

kinsim3 function:

```
void kinsim3( int Zb, int Zt, double Ab, double At,
    double thick /* mg/cm^2 */, double Eb /* MeV/u */,
    double dEb = 0.1 /* MeV/u */, double Ex = 1.0 /* MeV */,
    double res = 0.6 /* % */, double cd_dist = 28.0 /* mm */,
    bool flat = false /* angular distribution? */,
    long Nevts = 1E6, string srim_dir = "./srim" )
```

sjekk opp om energi fra online kalibrering passer med simuleringen.

```
$ cd ~/GitHub/MasterThesis/Scripts/plotting
$ root
root [0] .L ParticlePlot.cpp++
root [1] simulation_plot("setup_Sm.txt", 1)
... <showing output from script>
```

Tilbakemelding:

explain figure: Sm/Pb inner ring, Sm/Pb outer ring
simulation does not consider cross sections: in simulation all angles are equally probable. The corresponding figure from your data looks therefore quite different.

Appendix G shows the simulated energy for each ring of the CD, in addition to the fitted peaks of each ring.

Table 4.3 shows the mid strip CD angles in the laboratory frame for the front of the CD.

4.3.2 Online calibration of particle detector

Every year there is a campaign at ISOLDE, where the staff configures a settings-file if there are any changes in the setup system. In addition they run a cocktail beam composed of different isotopes on a specific target to make a calibration file containing the calibration coefficients for both the CD and γ -detectors. This calibration file is adjusted for each experiment following the campaign period. In this way it is easy to sort and analyze during the experiment if it is going well and to make preliminary Doppler-corrected γ -spectra.

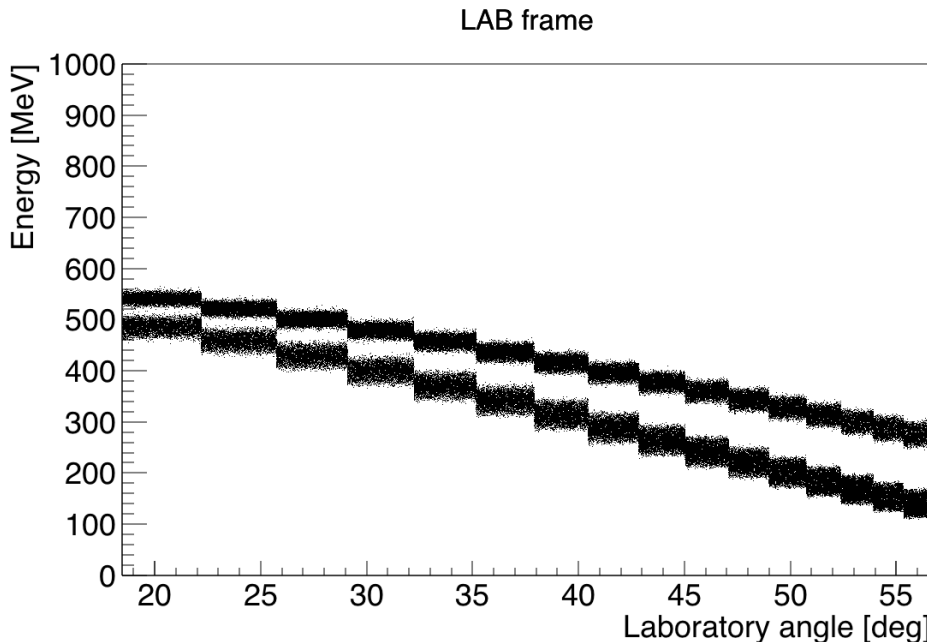


Figure 4.1: Simulation of the kinematics in the LAB frame for ^{140}Sm on ^{208}Pb at 4.65 MeV/u.

The settingsfile and calibration files used in this experiment can be found in `~/GitHub/MasterThesis/Miniball-config`, but when used with `MiniballCoulexSort` the default path is `~/GitHub/Miniball/MiniballCoulexSort/config`.

Trenger en overgang til M2R.

Just as for the `MedToRoot` program, I made a bash script named `Q4S.sh` for the `TreeBuilder` and `AQ4Sort` programs. `Q4S.sh` uses either `AQ4Sort` to make histograms for each pixel of the particle detector (used for calibration) or `Treebuilder` to build events, with a lot of files in one go for both. When using the online calibration, we don't need to use the `AQ4Sort` program, because we already have the calibration coefficients. They are adjusted in the beginning and during the experiment. `TreeBuilder` makes event trees and energy spectra for both particle and γ detection which can be used for analyzing the Coulomb excitation events. The `OnBeam.root`-files are loaded into `TreeBuilder` via `Q4S.sh` with the commands

```
$ cd ~/GitHub/MasterThesis/Scripts/sorting
$ ./Q4S.sh Sm online TB
... <showing output from script>
$ mv Sm_online-TreeBuilder-2019-06-24.root ../../Sorted_data/
```

I also made other helping scripts to get histograms, do fitting, comparison and calibration. After the sorting, I moved the file to a folder of sorted data (with the `mv` command), and gave the relative path in the `setup_Sm.txt` file in `Scripts/plotting/` used as input in the `ParticlePlot.cpp` script. This script has to be loaded into the ROOT 6 framework to extract the histograms of interest and fix the formatting. To run the `ParticlePlot.cpp` in interaction with ROOT, the following commands are used

```
$ cd ~/GitHub/MasterThesis/Scripts/plotting
$ root
root [0] .L ParticlePlot.cpp++
root [1] plot_front_back_energy("setup_Sm.txt", "online")
... <showing output from script>
```

[Figure 4.2](#) shows the back vs. front energy (online calibration) for the four different quadrants of the CD. The plots shows a part of a line for each front and back strip. An indication of a good calibration is when all detectors lie on a linear line ($y = x$), meaning that the front side and the back side of the CD has detected the same energy. From the figure we see that not all detectors fit the line, indicating that there are some calibration coefficients wrong in some of the strips. One major problem with the online calibration is that a number of the back strips have the wrong gains as shown in [Figure 4.4b](#).

4.3.3 User calibration of particle detector

My goal of the calibration was to make a program that could automatically fit the plots I needed, but it became more and more manual labor. In logarithmic scale (log-scale) the data looked more Gaussian distributed, but it is not the case in linear scale. For the centroids, it was very hard to tell in log-scale how precise the automatic fitting were. Because of the complex peak shapes, it is very hard to do an automatic fitting it seems. The peaks demands very much individual care. This I could not do with a automatic program. The downfall of the automatic "centroid collector" came when trying it on the secular strips of the CD. There is just too much individual differences to calibrate the secular strips with a simple script given a channel range for all 12 back strips. I found out this way to late. There isn't any range to rule them all, at least since the fitting function can behave very strange given a too small or too big range. To implement a proper automatic fitting program, one would have to find a function with a negatively (left) skewed distribution or negative skewness (right modal), where most of the data is more than the mean. Sadly I discovered this too late to implement it.

Honestly it might be better to simply hover the mouse over the correct "feature" of the peak, be it the centroid or the maximum, and compare that. The

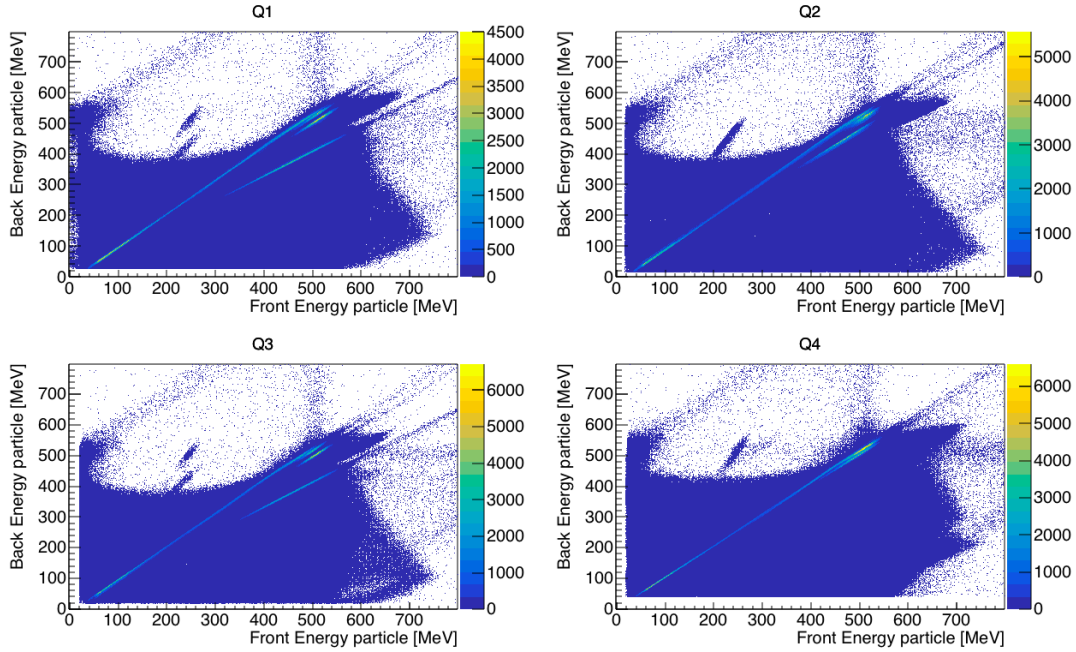


Figure 4.2: Online calibration for the CD showing the four quadrants. It generally looks quite good, but there is a number of the secular strips (back side) that have the wrong gains.

fitting just doesn't seem reliable.

In some spectra it is very hard to determine the centroid of the Pb peaks. We tried to use additional data from experiment IS553 (^{144}Ba on ^{58}Ni), which was right before our experiment. The reason for this was to try to get calibration for the lower energy spectra. But unfortunately the data from the IS553 experiment was a bad fit with our experiment. It gave a steeper slope than the online calibration, which was very good to begin with. Looking at the front vs. back energy plots, the diagonal lines are almost disappearing in the middle, and they are a lot broader than the online calibration. One big problem if I'm not using the Ni data, I cannot get any calibration coefficients for f16 and maybe f15 for Pb since they don't show much in the back detectors, even with many root-files together (we throw f1, because of the inner ring was totally broken, no change of splitting Pb from Sm). f2 was also a bit difficult for both Ni and Pb. It would have been nice with some low energy points and high energy points to calibrate as well. We also found something weird with Q4_b1, it shows a lot more counts than all the other back strips.

The total amount of annular strips to calibrate on the front side of the CD is 64 (4 quadrants \cdot 16 rings). On the back side we have 48 secular strips (4 quadrants \cdot 12 strips). To fully calibrate the CD, one need all the centroids of the peaks from both sides, 128 centroids (64 annular strips \cdot 2 peaks/ring) on the

front side and 1536 centroids ($48 \text{ secular strips} \cdot 2 \text{ peaks/ring} \cdot 16 \text{ rings}$) on the back side. The total centroids to collect are 1664 centroids, and this I did not want to do manually. For a quick calibration, or a bare minimum calibration, one needs two peaks in each annular strip and two peaks in each secular strip, making it 224 centroids. All above this just makes it more precise.

The innermost ring of the CD was very damaged by the bombardment of particles hitting it, so we had to remove the innermost ring from the data set (making the total centroids to collect to be 1500). In the innermost ring, it was impossible to separate the beam and target peak. This is unfortunate since the innermost ring has the most statistics, but Si detectors don't last forever. It was old and supposed to be changed after our experiment.

Excluding detector strips is easy, the only thing to do is to set gain and offset to -1. That will make the energy calibration negative, and fall out of the scope. It is the way it is usually done for dead CD strips or dead γ -detectors.

Changing the relative path in the *setup_Sm.txt* file used as input in the *ParticlePlot.cpp* script, we now have

```
$ cd ~/GitHub/MasterThesis/Scripts/sorting
$ ./Q4S.sh Sm user TB
... <showing output from script>
$ mv Sm_user-TreeBuilder-2019-06-20.root ../../Sorted_data/
```

TreeBuilder

```
$ ./Q4S.sh Sm user TB
____ TreeBuilder ____
input file(s):
... <shows a list of all input files>
output file: Sm_user-TreeBuilder-2019-06-20.root
calibration file: ../../Miniball-config/IS558-user.cal
WeightPR: 0.75
Particle distribution:
Q0 fired: 12243817
Q1 fired: 12277727
Q2 fired: 11479362
Q3 fired: 10936096
Finished .
```

AQ4Sort

```
$ ./Q4S.sh Sm user Q4
Info: No flag option for 'AQ4Sort'. Ignoring optional flag .
```

```
— AQ4Sort —
calibration file: ../../Miniball-config/IS558-user.cal
input file(s):
... <shows a list of all input files>
output file: Sm_user-AQ4Sort-2019-06-24.root
```

The user calibration of the CD shown in [Figure 4.3](#) is basically the online calibration without the innermost ring.

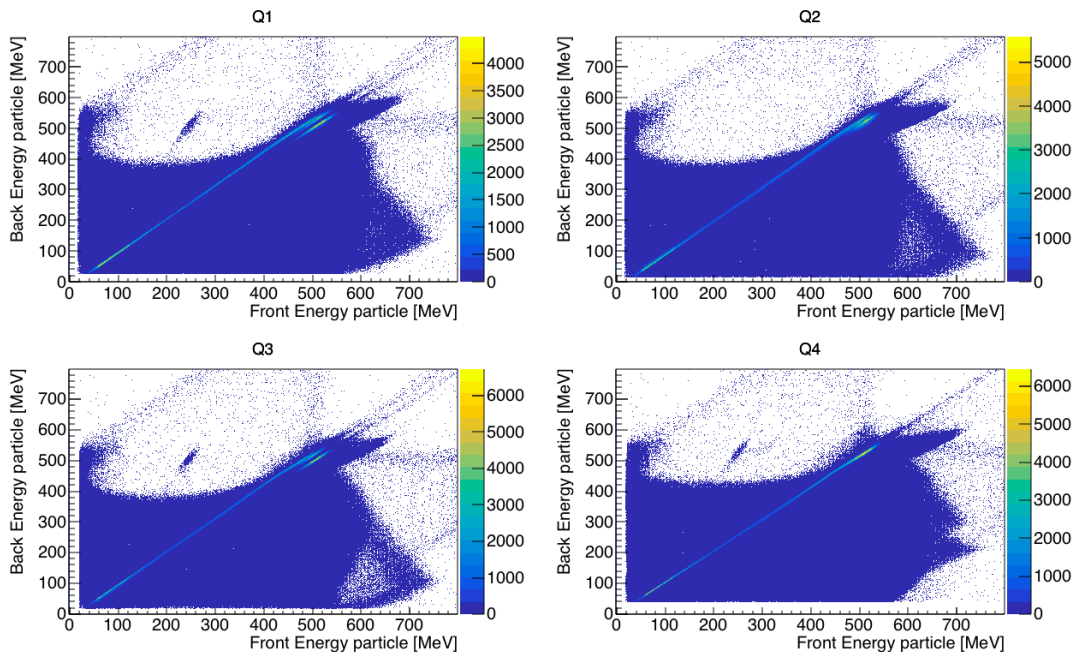


Figure 4.3: User calibration for the CD showing the four quadrants.

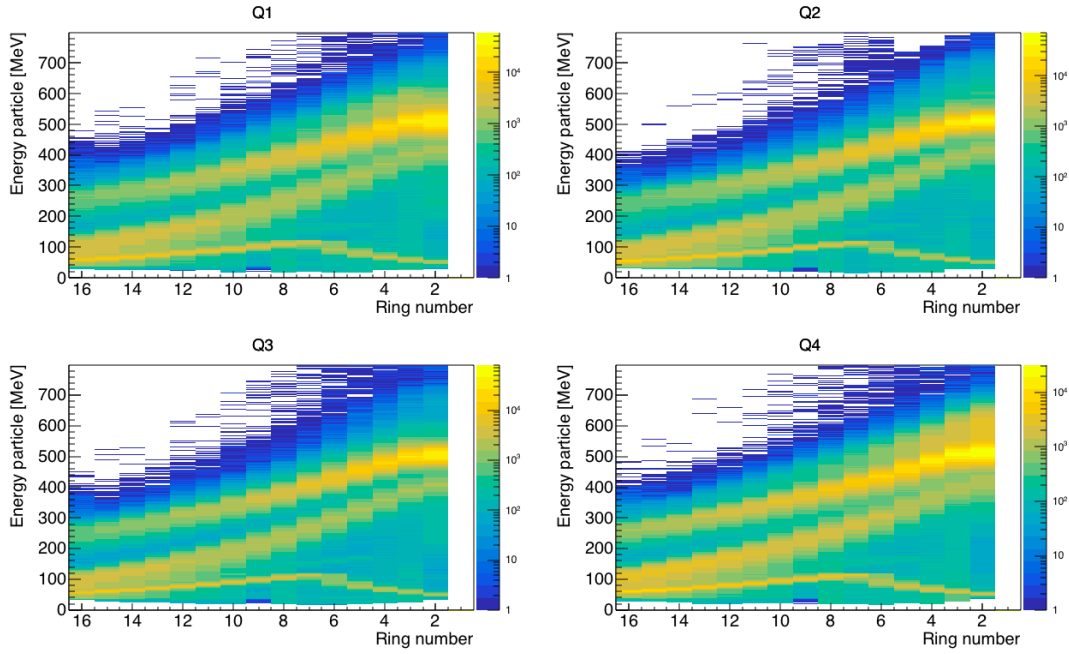
Back side:

Calibrating the back CD strips is the same as the front, however because they cover a large range of angles in the θ direction, we need to gate on one of the front strips to define an angle and therefore an energy. For this purpose, we will find the code `AQ4Sort` in the `TreeBuilder` directory. It operates the same files as `TreeBuilder` does, but with the purpose of making every combination of gates on front and back strips so that you have the front and back energy for every "pixel".

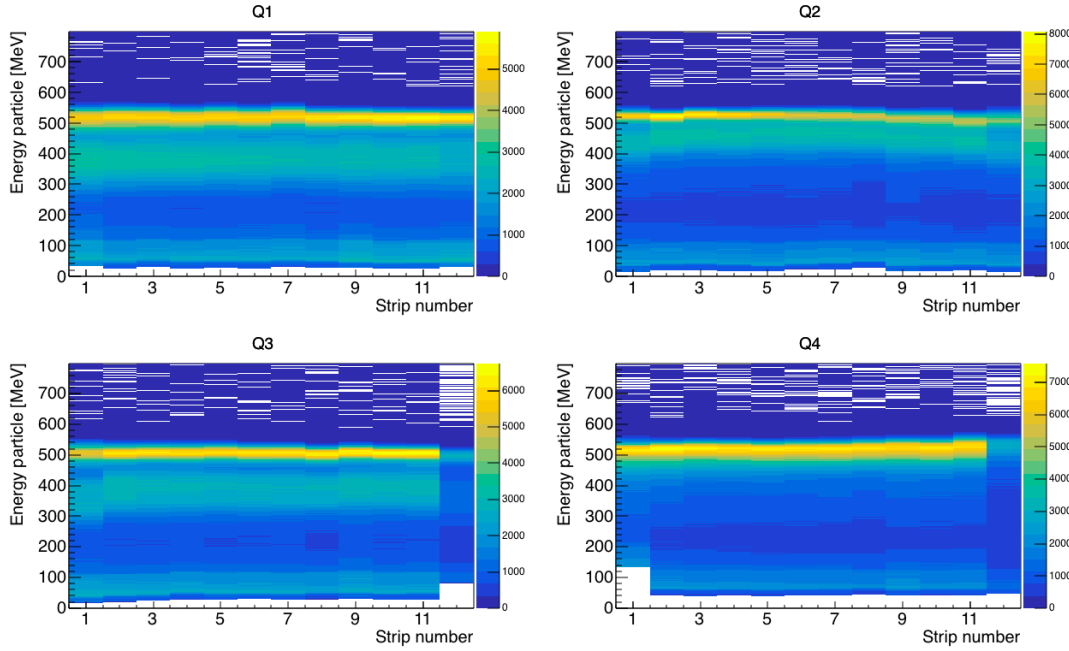
Notes

Simulation fit \rightarrow `Q4S_fit()` \rightarrow `particle-calibration.py` \rightarrow `ADC-generator.py` \rightarrow copy the calibration from the terminal and paste into calibration file

Visualize plots using ROOT and the scripts.



(a) CD front. Ring number 16 is the outermost ring and ring number 1 is the innermost ring.



(b) CD back. A number of the secular strips have the wrong gains.

Figure 4.4: Energy vs. strip number for each quadrant of the CD.

ADC:

annular (front) strip ID of particle (0 = outer; 15 inner)
secular (back) strip ID of particle (0 to 12; clockwise wrt beam)

ROOT: analysere data [36]

My scripts: `ParticleFit.cpp`, `GammaFit.cpp`, `ParticlePlot.cpp`, `GammaPlot.cpp`,
++ (python, bash,..)

4.3.4 Threshold

The continuum of events at low energy comes from charge sharing between the strips. [Figure 4.5](#) shows the big peak of the charge sharing on the front and back side. This peak we call the "pedestal", because it is like a massive statue in front of the interesting data. For the very heavy ions, the total amount of charge deposited gets split between neighboring strips of the CD.

There is a single common gate for each ADC, containing channels from one CD quadrant. Therefore, when there is an event in one strip of the CD all channels are readout, but the channels without a real event read a "zero" energy. These are the events in the pedestal. One should define the threshold for each ADC channel to be above this peak. After a correct calibration is applied, this pedestal will be calibrated out of the physical energy range.

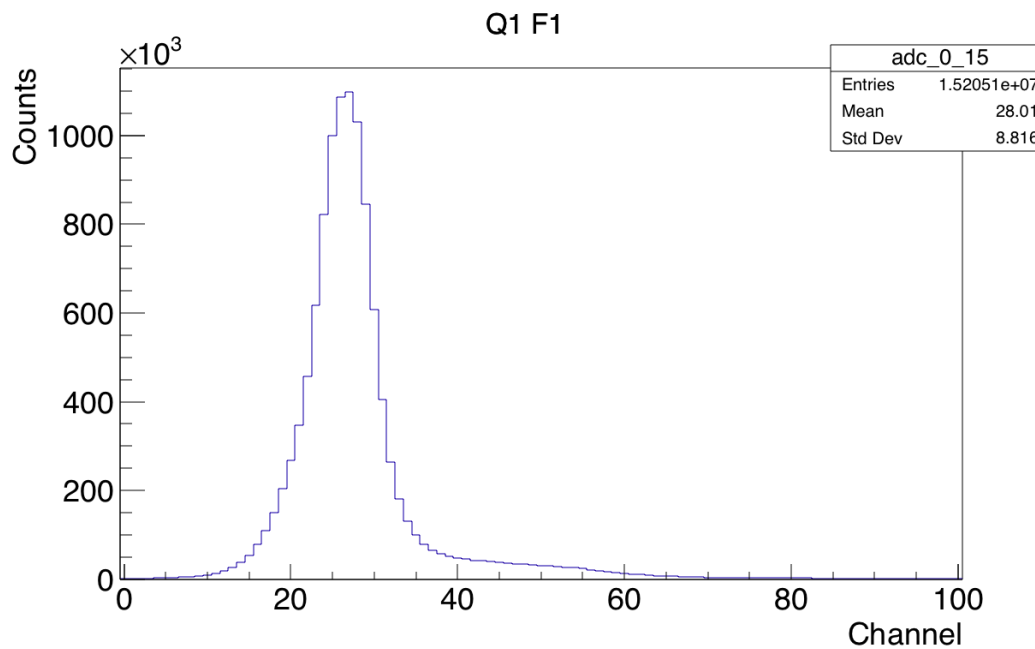
MiniballCoulexSort does perform some tricks to try to recover the correct energy and position, but that depends on counting the number of strips that fire. We use a software threshold to cut away the pedestal. If the threshold is set too low, we will include "pedestal" events and it will get things wrong. If the threshold is too high, we will miss some events that have charge sharing and get the wrong energy for the particle. It is easier to set thresholds in linear scale than logarithmic, because in logarithmic scale the threshold value will decrease very much and it's hard to see where to set the limit. The default threshold (if none is given in the calibration file) is set to channel 100. In some cases this is too much and in others this is not enough. For each ADC channel, the threshold can, and should be set. [Figure 4.6](#) shows the software threshold set in the calibration file on the front and back side for one strip on each side.

Goal: You are not including the pedestal, and you don't cut away too many events from the continuum.

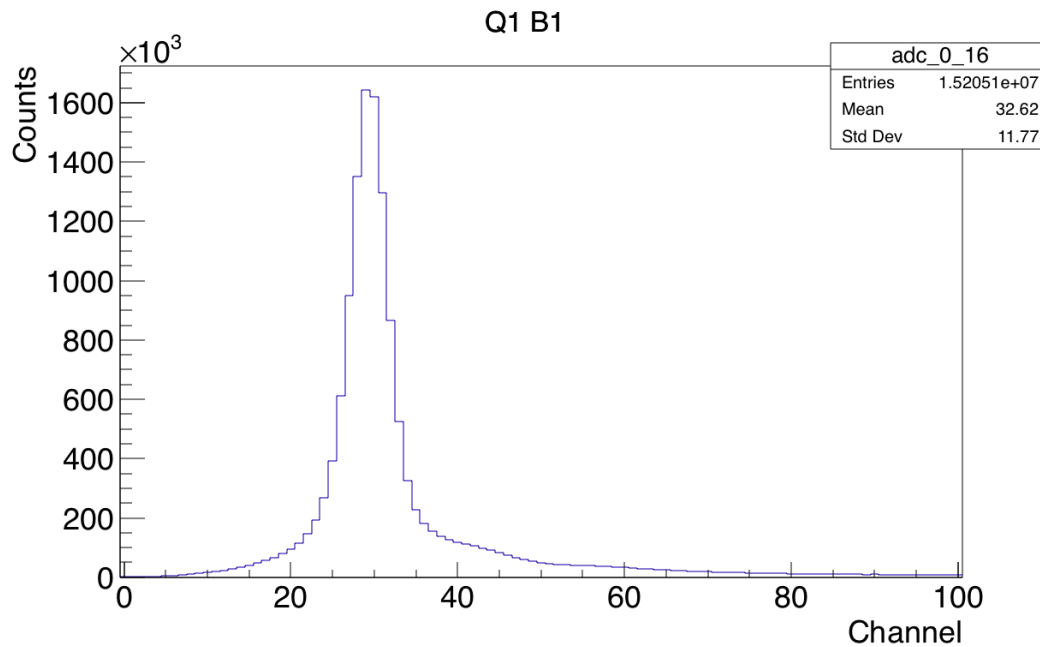
Tilbakemelding:

I presume that charge sharing is only considered if 2 firing strips are neighbors?

The key spectra to look at are [Figure 4.7](#) and [Figure 4.8](#). [Figure 4.8](#) shows how many particles have strips fired on the front side or back side of the CD. The debug IDs are explained by [Table 4.4](#). If we have too many debug ID = 3, then the threshold is too low. If we have a large continuum/background in



(a) Pedestal in quadrant 1, annular strip 1.



(b) Pedestal in quadrant 1, secular strip 1.

Figure 4.5: The pedestal from charge sharing in the front and back side of the CD.

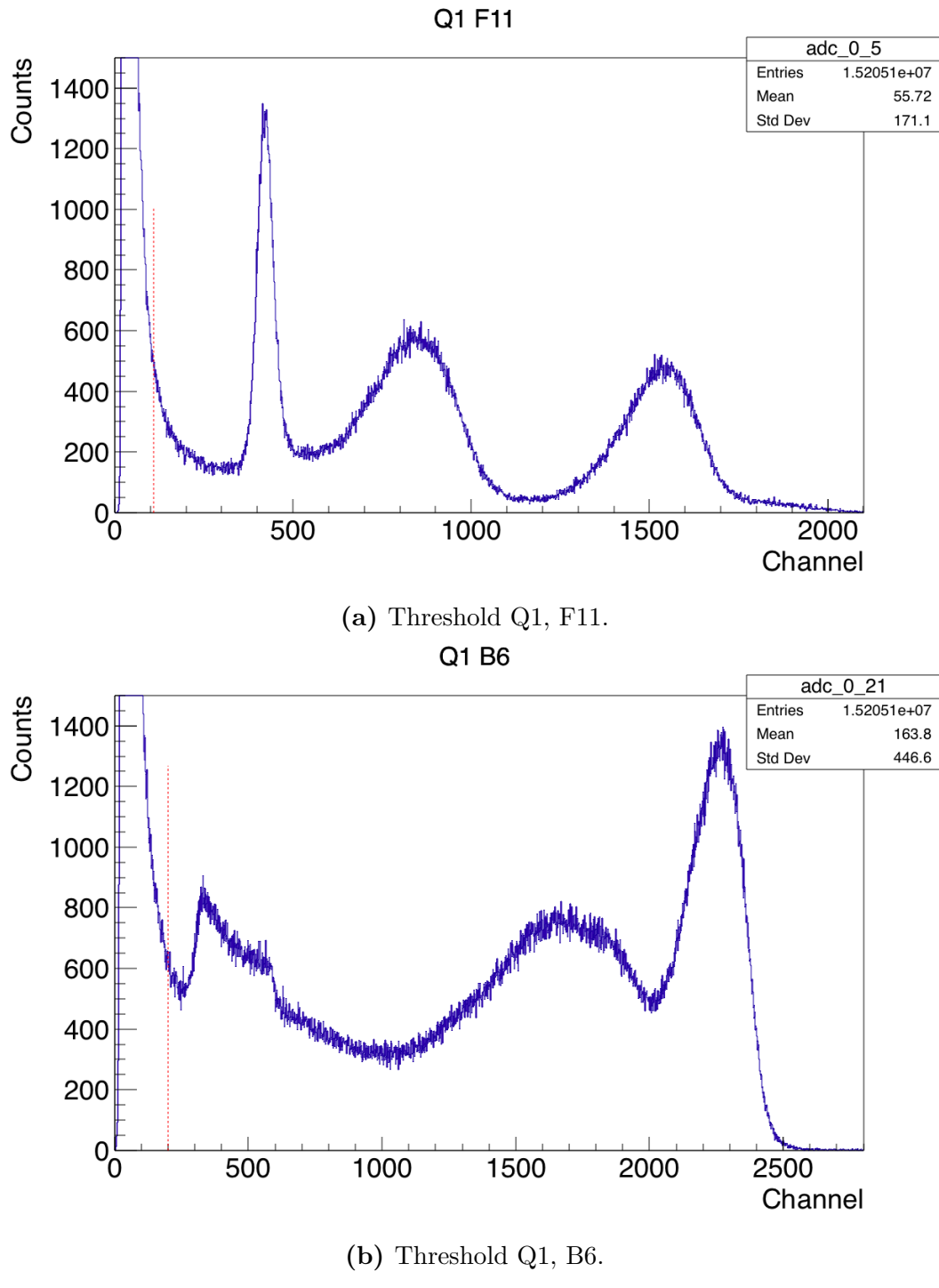


Figure 4.6: ??

[Figure 4.7](#), the thresholds are too high. The best thing to do is to play about with different values to see what is best. Debug ID 20 is when no particle can be found, because there is no energy registered in either the front or the back strips. This can only happen when the front energy is below the software threshold set by the user in the calibration file and the back energy is either in a broken strip or is also below the software threshold. It is likely that it is some noise events or charge sharing that comes below the threshold.

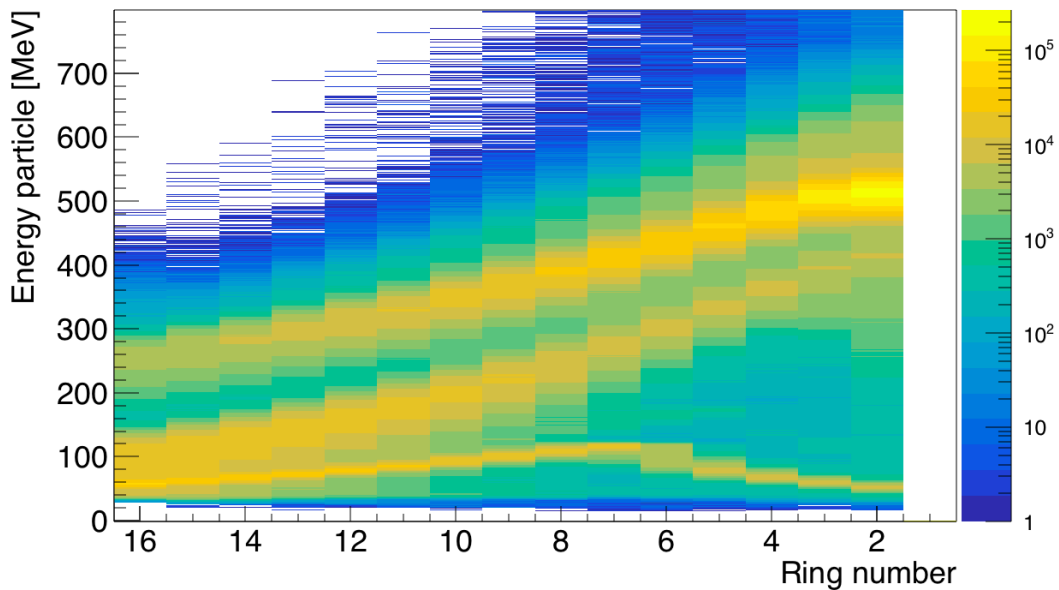


Figure 4.7: Energy vs. ring number.

4.3.5 Time calibration

Using the `ParticlePlot.cpp` script, the ADC time offsets can be extracted by the following commands

```
$ cd /Users/trondwj/GitHub/MasterThesis/Scripts/plotting
$ root
root [0] .L ParticlePlot.cpp++
root [1] check_ADC_time_offsets("setup_Sm.txt")
```

or they can be manually reached by

```
$ cd /Users/trondwj/GitHub/MasterThesis/Sorted_data
$ root Sm_user_TreeBuilder-2019-04-10.root
root [1] new TBrowser()
```

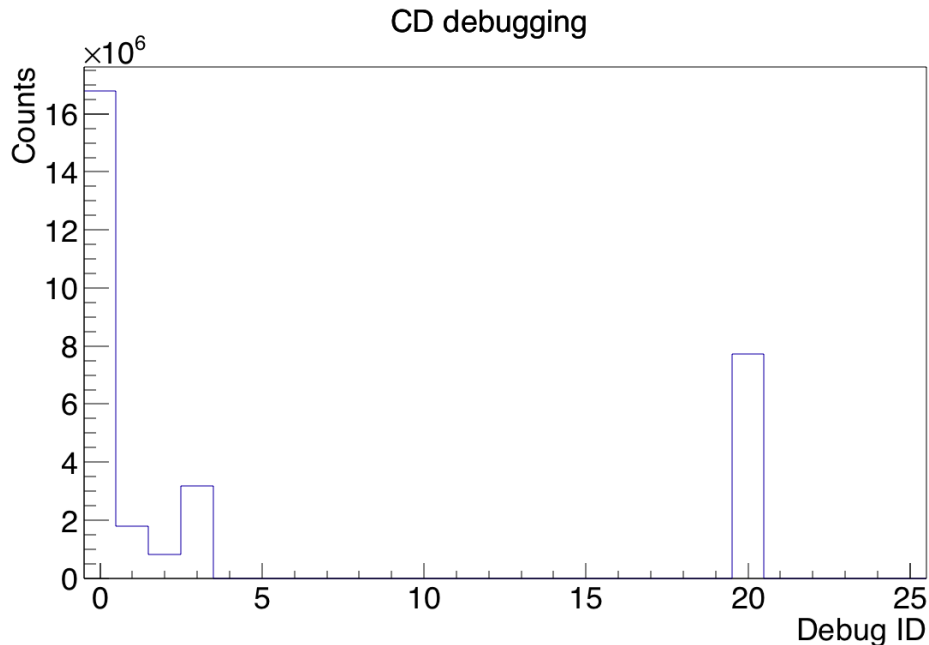


Figure 4.8: CD debugging. Debug IDs are explained by [Table 4.4](#).

and in the browser, the histograms named `tdiff_gp_i` (where i is a number between 0 and 3) will lie under all the folders. The peaks of these plots have the interesting x-value. Zooming into the peaks, it is very clear what value it is. These values are provided in the calibration file under ADC time offsets (ticks). These values can change depending on the amount of data sorted, so it is wise to double check them.

After the peak values have been collected, they should be written into the calibration file

```
# ADC time offsets (ticks)
adc_0.TimeOffset: 0
adc_1.TimeOffset: -2
adc_2.TimeOffset: -3
adc_3.TimeOffset: 5
```

Tilbakemelding:
one time spectrum per quadrant?

HUSK: Si noe om ADC time offsets + Threshold. Og at man må se på det tidlig, så resortere.

`M2R.sh` → `Q4S.sh` → check time offset → threshold → `Q4S_fit()` → `particle-calibration.py` → `ADC-generator.py` → copy the calibration from the terminal and paste into calibration file

Tilbakemelding:

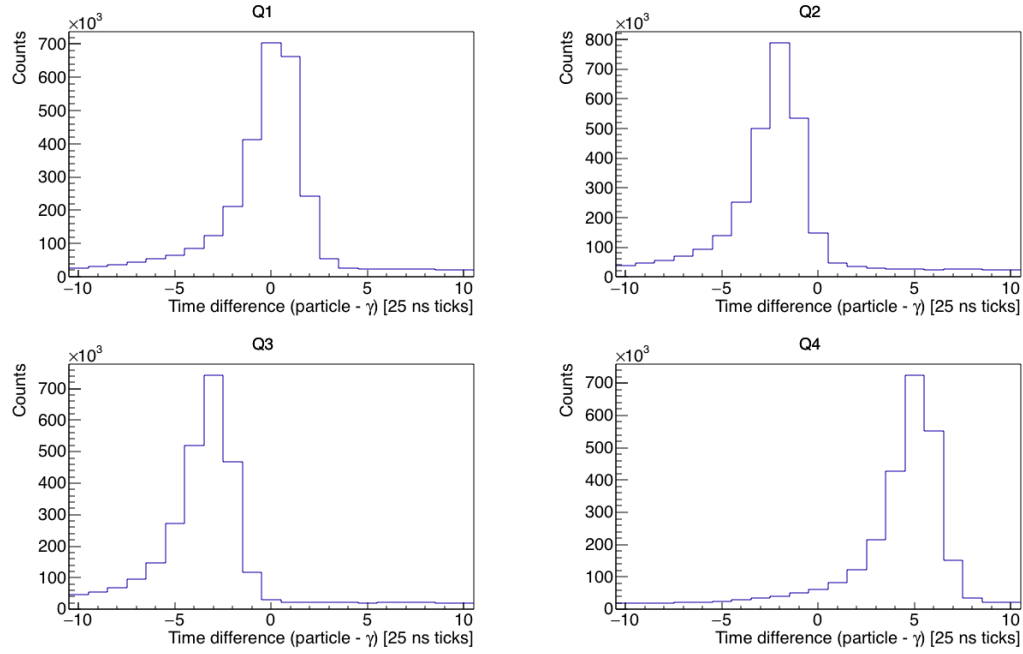


Figure 4.9: ADC time offsets for the four quadrants of the CD.

need to explain the time spectra: start - stop

purpose: align time spectra so that you can set a prompt time gate.

→ correlate γ -rays with particles.

OBS:

After the threshold and ADC time offsets are set, we must rerun the TreeBuilder step with the updated calibration file.

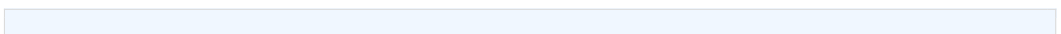
4.3.6 Gamma

Calibration of the γ detectors

The nominal calibration will be quite good for most detectors in a certain energy range, because it is designed to be that way. The gains of each DGF are matched during the setup of the experiment so that the online analysis is more straightforward. However, there are non-linearities and drifting offsets and gains over time that have to be corrected for with a proper calibration using the $^{133}\text{Ba}/^{152}\text{Eu}$ source data.

DGF: Digital γ finder
addback, singles, ...

CLXAna



```
$ ./Coulex.sh -n
--- Coulex: normal ---
Input parameters:
Zb = 62
Ab = 140
Zt = 82
At = 208
Eb = 4650 keV/u
Ex = 531 keV
thick = 1.4 mg/cm2
depth = 0.7 mg/cm2
cddist = 26.98 mm
cdoffset = 242.6 degrees
deadlayer = 0.0007 mm
contaminant = -1 mg/cm2
spededist = 23.6 mm
bg_frac = -0.75
srim = /Users/trondwj/GitHub/MasterThesis/SRIM
cutfile = ../../Sorted_data/outputfile.root:Bcut:Tcut
Begin g_clx loop.
Info in <TCanvas::Print>: pdf file /Users/trondwj/GitHub/
    MasterThesis/SRIM/140Sm_208Pb.pdf has been created
Info in <TCanvas::Print>: pdf file /Users/trondwj/GitHub/
    MasterThesis/SRIM/208Pb_208Pb.pdf has been created
Info in <TCanvas::Print>: pdf file /Users/trondwj/GitHub/
    MasterThesis/SRIM/140Sm_Si.pdf has been created
Info in <TCanvas::Print>: pdf file /Users/trondwj/GitHub/
    MasterThesis/SRIM/208Pb_Si.pdf has been created
Initialising histograms...
Looping over events...
Warning in <TClass::Init>: no dictionary for class trevts is
    available
1-particle events = 89020258%
Finished.
```

hadd (from ROOT)

After saving "part" from CLXAna-file:

```
$ cd GitHub/ROOT-framework/build/bin
$ hadd /Users/trondwj/GitHub/MasterThesis/Sorted_data/
    outputfile.root /Users/trondwj/GitHub/MasterThesis/
    Sorted_data/part.root /Users/trondwj/GitHub/MasterThesis/
    Sorted_data/Bcut.root /Users/trondwj/GitHub/MasterThesis/
    Sorted_data/Tcut.root
```

particle-gamma and particle-gamma-gamma coincidence

Gamma:
 core ID from 0 to 23
 segment ID from 0 to 6 (zero is the core)
 cluster ID from 0 to 7

The Miniball spectrometer [13]
 p. 8:

Efficiency and resolution: left bottom:

The application of an add-back (AB) routine involves the summing of the energies of two coincident gamma rays within 100 ns in neighboring cores on the same cluster detector. This situation corresponds to a Compton-scattered γ -ray event where the energy of the γ -ray is shared between two or more crystals in the same triple cluster detector. For higher-energy γ -rays, where scattering from one crystal into its neighbor is quite likely, this improves the efficiency, but for low-energy γ -rays, where scattering is less likely, summing effects actually reduce the efficiency. For this reason a cut-off is normally applied and AB is only performed for energies above this threshold.

4.3.7 Doppler correction

From `offl_root_med.pdf`

"Direction of the central axis of the detector (r, θ, ϕ) and the notation about the axis of the cluster (α), **is this correct??**. Needed to calculate the positions of the segments or the position of a point determined by the pulse-shape analysis.

In order to perform the Doppler shift, we need to know the angle in the Miniball frame of reference of the interaction point. We determine the interaction point either from the segment with the largest energy or using pulse-shape analysis. In the former case, we need to know the position of the centre of each segment. In the latter, we need geometrical information to relate the time-to-steepest slope and ratio of the mirror charge amplitudes to the angle between the interaction point, the target and the emitted particle."

Notes

For Miniball geometry (angles) [41].

4.4 Data analysis

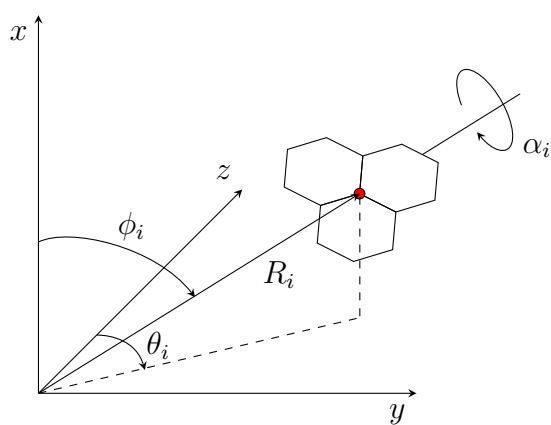


Figure 4.10: Miniball angles, where i denotes cluster number from [Table 4.6](#).

Table 4.1: ADC wiring for Coulomb excitation experiments.

| ADC | Quadrant | Channel | Front strip [F] or back strip [B] |
|-------|----------|---------|--------------------------------------|
| 0 - 3 | 1 - 4 | 0 | F |
| 0 - 3 | 1 - 4 | 1 | F |
| 0 - 3 | 1 - 4 | 2 | F |
| 0 - 3 | 1 - 4 | 3 | F |
| 0 - 3 | 1 - 4 | 4 | F |
| 0 - 3 | 1 - 4 | 5 | F |
| 0 - 3 | 1 - 4 | 6 | F |
| 0 - 3 | 1 - 4 | 7 | F |
| 0 - 3 | 1 - 4 | 8 | F |
| 0 - 3 | 1 - 4 | 9 | F |
| 0 - 3 | 1 - 4 | 10 | F |
| 0 - 3 | 1 - 4 | 11 | F |
| 0 - 3 | 1 - 4 | 12 | F |
| 0 - 3 | 1 - 4 | 13 | F |
| 0 - 3 | 1 - 4 | 14 | F |
| 0 - 3 | 1 - 4 | 15 | F |
| 0 - 3 | 1 - 4 | 16 | B |
| 0 - 3 | 1 - 4 | 17 | B |
| 0 - 3 | 1 - 4 | 18 | B |
| 0 - 3 | 1 - 4 | 19 | B |
| 0 - 3 | 1 - 4 | 20 | B |
| 0 - 3 | 1 - 4 | 21 | B |
| 0 - 3 | 1 - 4 | 22 | B |
| 0 - 3 | 1 - 4 | 23 | B |
| 0 - 3 | 1 - 4 | 24 | B |
| 0 - 3 | 1 - 4 | 25 | B |
| 0 - 3 | 1 - 4 | 26 | B |
| 0 - 3 | 1 - 4 | 27 | B |
| 0 - 3 | | 28 | Empty |
| 0 - 3 | | 29 | Empty |
| 0 - 3 | | 30 | Empty |
| 0 - 3 | 1 - 4 | 31 | PAD |
| 4 | | 0 | Ionization Chamber |
| 4 | | 1 | Ionization Chamber |

Table 4.2: The naming of histograms from `TreeBuilder` vs. `AQ4Sort`.

| Quadrant | Front strip [F] or back strip [B] | TreeBuilder | AQ4Sort |
|----------|--------------------------------------|-------------|-----------|
| 1 | F 15 | adc_0_0 | fE_Q1_f1 |
| 1 | F 14 | adc_0_1 | fE_Q1_f2 |
| 1 | F 13 | adc_0_2 | fE_Q1_f3 |
| : | : | : | : |
| 1 | F 1 | adc_0_14 | fE_Q1_f15 |
| 1 | F 0 | adc_0_15 | fE_Q1_f16 |
| 1 | B 0 | adc_0_16 | bE_Q1_b1 |
| 1 | B 1 | adc_0_17 | bE_Q1_b2 |
| 1 | B 2 | adc_0_18 | bE_Q1_b3 |
| : | : | : | : |
| 1 | B 11 | adc_0_26 | bE_Q1_b11 |
| 1 | B 12 | adc_0_27 | bE_Q1_b12 |
| 2 | F 15 | adc_1_0 | fE_Q2_f1 |
| : | : | : | : |
| 2 | F 0 | adc_1_15 | fE_Q2_f16 |
| 2 | B 0 | adc_1_16 | bE_Q2_b1 |
| : | : | : | : |
| 2 | B 12 | adc_1_27 | bE_Q2_b12 |
| 3 | F 15 | adc_2_0 | fE_Q3_f1 |
| : | : | : | : |
| 3 | F 0 | adc_2_15 | fE_Q3_f16 |
| 3 | B 0 | adc_2_16 | bE_Q3_b1 |
| : | : | : | : |
| 3 | B 12 | adc_2_27 | bE_Q3_b12 |
| 4 | F 15 | adc_3_0 | fE_Q4_f1 |
| : | : | : | : |
| 4 | F 0 | adc_3_15 | fE_Q4_f16 |
| 4 | B 0 | adc_3_16 | bE_Q4_b1 |
| : | : | : | : |
| 4 | B 12 | adc_3_27 | bE_Q4_b12 |

Table 4.3: Mid ring CD angles in laboratory frame with distance from target to CD of 26.98 mm. Ring 1 is the innermost ring and ring 16 is the outermost ring. The centroid energy is from simulation with `kinsim3`. E_t is the energy of the target particle and E_b is the energy of the beam particle.

| Ring number | Mid ring distance [mm] | Angle [°] | E_t [MeV] | E_b [MeV] |
|-------------|------------------------|-----------|-------------|-------------|
| 1 | 10 | 20.3 | 484.86 | 539.89 |
| 2 | 12 | 24.0 | 457.53 | 520.55 |
| 3 | 14 | 27.4 | 428.87 | 499.72 |
| 4 | 16 | 30.7 | 398.95 | 478.33 |
| 5 | 18 | 33.7 | 369.54 | 456.71 |
| 6 | 20 | 36.5 | 340.64 | 435.42 |
| 7 | 22 | 39.2 | 313.65 | 414.84 |
| 8 | 24 | 41.7 | 287.31 | 395.31 |
| 9 | 26 | 43.9 | 262.77 | 376.35 |
| 10 | 28 | 46.1 | 240.36 | 358.75 |
| 11 | 30 | 48.0 | 219.53 | 342.40 |
| 12 | 32 | 49.9 | 198.95 | 326.87 |
| 13 | 34 | 51.6 | 182.41 | 312.31 |
| 14 | 36 | 53.1 | 164.55 | 299.11 |
| 15 | 38 | 54.6 | 151.51 | 286.78 |
| 16 | 40 | 56.0 | 139.62 | 273.80 |

Table 4.4: CD debugging.

| CD debug ID | Strips fired | |
|-------------|-------------------|-----------|
| | Front side | Back side |
| 0 | 1 | 1 |
| 1 | 1 | 2 |
| 2 | 2 | 1 |
| 3 | >1 | >1 |
| 20 | No particle found | |

Table 4.5: DGF

| Cluster | Segment | Channel | Name |
|---------|---------|---------|------|
| 0 - 3 | 1 - 4 | 0 | |

Table 4.6: Geometry to the center of the Miniball HPGe clusters (red dot in [Figure 4.10](#)) for the Doppler correction.

| Cluster | θ_i [°] | ϕ_i [°] | α_i [°] | R_i [mm] |
|---------|----------------|--------------|----------------|------------|
| 0 | 311.16 | 126.67 | 129.79 | 107.08 |
| 1 | 51.08 | 62.74 | 51.83 | 100.59 |
| 2 | 309.02 | 126.87 | 51.23 | 105.76 |
| 3 | 251.90 | 57.44 | 130.31 | 105.40 |
| 4 | 296.93 | 235.53 | 128.74 | 106.48 |
| 5 | 233.45 | 239.09 | 46.67 | 105.18 |
| 6 | 59.42 | 308.67 | 131.04 | 127.04 |
| 7 | 130.56 | 309.09 | 46.46 | 110.18 |

Chapter 5

Experimental results

Very pure beam (did we have statistics of this?) - resultat til avhandling. sjekk etter doppler-korrigering. Nd-contaminasjon? i så fall veldig lite, 1-2 prosent?

Tilbakemelding:

we would have to look at the γ -spectra to identify any contaminants. There may be a little bit of Nd-140 in the beam, but if so, it is very little (judging from on-line spectra).

Chapter 6

Discussion

Level scheme (from Klintefjord?)

Tilbakemelding:

at some point you should show the level scheme.

- motivation: to explain what is known, and which transition probabilities you want to measure.

Perhaps also to explain what theory predicts.

- discussion: if you get γ -spectrum for $^{140}\text{Sm} \rightarrow$ to explain what you see.

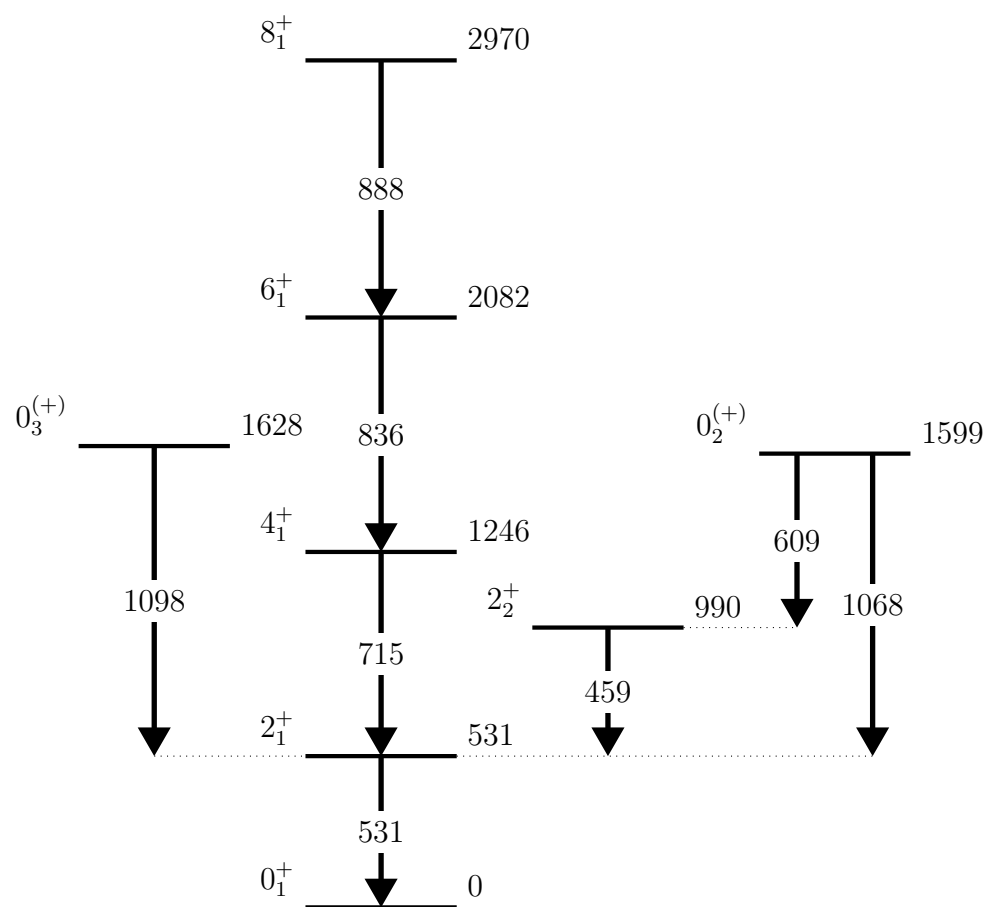


Figure 6.1: Level scheme for ^{140}Sm . Adapted from Klintefjord.

Chapter 7

Summary and outlook

Future work: Better calibration of particle detectors and γ -detectors (online not perfect). Take into account the shape of the peaks \implies calibrate the particle detectors manually.. Takes a lot of time! But maybe less than trying to fit all in a script? Had I just known...

Efficiency calibration ++

Fra oppgaveteksten:

determine Coulomb excitation yields. These yields will then, in a second step, be compared to theoretical calculations and transition probabilities and quadrupole moments will be extracted using chi-square minimization procedures.

GOSIA and GOSIA2 analysis?

https://www.pas.rochester.edu/~cline/Gosia/Gosia_Manual_20110609.pdf

Appendices

Appendix A

Symbol list

Table A.1: Table of symbols with explanations.

| $T_{1/2}$ | Half-life |
|-----------|-----------|
|-----------|-----------|

Appendix B

Acronyms and abbreviations

Table B.1: Table of acronyms and abbreviations.

| | |
|----------------------------------|--|
| ADC | Analog to Digital Converter |
| bash | Bourne-Again SHell |
| CERN | European Council for Nuclear Research (in French: Conseil Européen pour la Recherche Nucléaire) |
| CD | Compact Disc |
| COULEX | COULomb EXcitation |
| DAQ | Data AcQuisition |
| DGF | Digital Gamma Finder |
| DSSSD | Double Sided Silicon Strip Detector (also known as CD) |
| GPS | General Purpose Separator |
| HRS | High Resolution Separator |
| HIE-ISOLDE | High Intensity and Energy upgrade at ISOLDE |
| HPGe | High Purity Germanium |
| ISOL | Isotope Separator On Line |
| ISOLDE | ISOL DEvice |
| LINAC | LINear ACcelerator |
| MBS | Multi Branch System |
| MED | MBS Event Data (also known as Miniball Event Data) |
| MAR _a BQ _U | MBS And ROOT Based Online/Offline Utility |
| PSB | Proton Synchrotron Booster |
| REX | Radioactive beam EXperiment |
| EBIS | Electron Beam Ion Source |
| REXEIBIS | Radioactive beam EXperiment Electron Beam Ion Source |
| REXTRAP | Radioactive beam EXperiment TRAP |
| REX-ISOLDE | Radioactive beam EXperiment at ISOLDE |
| RIB | Radioactive Ion Beam |
| RILIS | Resonance Ionization Laser Ion Source |
| SRIM | Stopping and Range of Ions in Matter |
| TDC | Time to Digital Converter |

Appendix C

Computer setup and environment

Some calibration code is based on the codes of Ville Virtanen and Dr. Liam Gaffney. Other code/scripts have been written by the author in C++ / Python.

C.1 The computer

The *MiniballCoulxSort* code does not require any a lot of computing power to run. [Table C.1](#) shows the computer with specifications used for the sorting and data analysis. Since the data from the experiment takes up about 60 GB, the limitation was with the SSD¹. When running the sorting and event-building programs, the space on the computer rapidly vanishes.

Table C.1: Computer used for sorting and data analysis.

| | |
|-----------|--|
| Model | MacBook Air (13-inch, 2017) |
| OS | macOS High Sierra (Version 10.13.6) |
| Processor | 1.8 GHz (Intel Core i5, dual core, 4 threads) Max turbo frequency: 2.90 Ghz |
| Memory | 8 GB (1600 MHz DDR3) |
| SSD | 128 GB |

C.2 The environment

Nevn den relative mappstrukturen, slik at terminal-commandoer gir mening. Både for Miniball kode og ROOT framework.

¹The SSD (solid-state drive) is the internal storage device in the computer.

```
/Users/trondwj/GitHub/Miniball/MiniballCoulexSort
```

```
/Users/trondwj/GitHub/Miniball/kinsim
```

```
/Users/trondwj/GitHub(ROOT-framework/build
```

C.3 Run time

TODO: Run timing on M2R.sh

Table C.2: Run time for building event trees. The run time of the bash scripts was timed with the built in command line script named `time`. It depends on the number of files added for tree building.

| Executable | Run time [min] |
|-------------|----------------|
| TreeBuilder | ~ 45 |
| AQ4Sort | ~ 130 |

Appendix D

Two-particle collision

D.1 Laboratory (LAB) frame of reference

The angles of the two-particle collision in the laboratory frame from [Figure 2.1a](#) is calculated in this section. A general approach is used to make it easier to hold track of the parameters. From the figure we can express the velocities as

$$\begin{aligned}\mathbf{u} &= \mathbf{u}_1 = u\hat{\mathbf{x}} \\ \mathbf{u}_2 &= 0 \\ \mathbf{v}_b &= \mathbf{v}_1 = v_1(\cos\theta\hat{\mathbf{x}} + \sin\theta\hat{\mathbf{y}}) \\ \mathbf{v}_t &= \mathbf{v}_2 = v_2(\cos\varphi\hat{\mathbf{x}} - \sin\varphi\hat{\mathbf{y}})\end{aligned}\tag{D.1}$$

where \mathbf{u}_1 and \mathbf{v}_1 is the initial and final velocity of the projectile $m_b = m_1$ respectively, and \mathbf{u}_2 and \mathbf{v}_2 is the initial and final velocity of the target $m_t = m_2$ respectively. The angles $\theta_b = \theta$ and $\theta_t = \varphi$ are the projectile and target angle respectively. We also introduce a ratio of the projectile mass to the target mass, $\alpha = m_1/m_2$.

Conservation of momentum gives

$$m_1\mathbf{u}_1 = m_1\mathbf{v}_1 + m_2\mathbf{v}_2$$

which in x-direction can be expressed as

$$\begin{aligned}m_1u &= m_1v_1 \cos\theta + m_2v_2 \cos\varphi \\ m_1(u - v_1 \cos\theta) &= m_2v_2 \cos\varphi \\ \frac{m_1}{m_2}(u - v_1 \cos\theta) &= v_2 \cos\varphi \\ \alpha(u - v_1 \cos\theta) &= v_2 \cos\varphi\end{aligned}\tag{D.2}$$

and in y-direction can be expressed as

$$\begin{aligned} 0 &= m_1 v_1 \sin \theta - m_2 v_2 \sin \varphi \\ m_1 v_1 \sin \theta &= m_2 v_2 \sin \varphi \\ \frac{m_1}{m_2} v_1 \sin \theta &= v_2 \sin \varphi \\ \alpha v_1 \sin \theta &= v_2 \sin \varphi \end{aligned} \quad (\text{D.3})$$

Conservation of energy gives

$$\begin{aligned} \frac{1}{2} m_1 \mathbf{u}_1^2 &= \frac{1}{2} m_1 \mathbf{v}_1^2 + \frac{1}{2} m_2 \mathbf{v}_2^2 \\ \frac{1}{2} m_1 (u^2 - v_1^2) &= \frac{1}{2} m_2 v_2^2 \\ \frac{m_1}{m_2} (u^2 - v_1^2) &= v_2^2 \\ \alpha (u^2 - v_1^2) &= v_2^2 \end{aligned} \quad (\text{D.4})$$

We now have three equations (Equation (D.2) - Equation (D.4)) with four unknown quantities ($v_1, \theta, v_2, \varphi$). Using the target angle φ as an independent variable, we can find expressions for the other three variables.

Squaring Equation (D.2)

$$\begin{aligned} \alpha^2 (u - v_1 \cos \theta)^2 &= v_2^2 \cos^2 \varphi \\ \alpha^2 (u^2 - 2uv_1 \cos \theta + v_1^2 \cos^2 \theta) &= v_2^2 \cos^2 \varphi \end{aligned}$$

and Equation (D.3)

$$\alpha^2 v_1^2 \sin^2 \theta = v_2^2 \sin^2 \varphi$$

and adding them together gives

$$\begin{aligned} \alpha^2 (u^2 - 2uv_1 \cos \theta + v_1^2 \cos^2 \theta + v_1^2 \sin^2 \theta) &= v_2^2 (\cos^2 \varphi + \sin^2 \varphi) \\ \alpha^2 (u^2 - 2uv_1 \cos \theta + v_1^2) &= v_2^2 \\ \alpha^2 u^2 - 2\alpha^2 uv_1 \cos \theta + \alpha^2 v_1^2 &= v_2^2 \\ \alpha^2 v_1^2 &= -\alpha^2 u^2 + 2\alpha^2 uv_1 \cos \theta + v_2^2 \\ \alpha^2 v_1^2 &= -\alpha^2 u^2 + 2\alpha u (\alpha v_1 \cos \theta) + v_2^2 \end{aligned} \quad (\text{D.5})$$

From Equation (D.2) we have

$$\begin{aligned} \alpha(u - v_1 \cos \theta) &= v_2 \cos \varphi \\ \alpha u - \alpha v_1 \cos \theta &= v_2 \cos \varphi \\ \alpha v_1 \cos \theta &= \alpha u - v_2 \cos \varphi \end{aligned} \quad (\text{D.6})$$

Substituting for [Equation \(D.6\)](#) into [Equation \(D.5\)](#) we get

$$\begin{aligned}\alpha^2 v_1^2 &= -\alpha^2 u^2 + 2\alpha u(\alpha u - v_2 \cos \varphi) + v_2^2 \\ \alpha^2 v_1^2 &= -\alpha^2 u^2 + 2\alpha^2 u^2 - 2\alpha u v_2 \cos \varphi + v_2^2 \\ \alpha^2 v_1^2 &= \alpha^2 u^2 - 2\alpha u v_2 \cos \varphi + v_2^2\end{aligned}\quad (\text{D.7})$$

Using [Equation \(D.4\)](#) we get

$$\begin{aligned}\left(\frac{\alpha}{\alpha}\right) \alpha(u^2 - v_1^2) &= v_2^2 \\ \alpha^2(u^2 - v_1^2) &= \alpha v_2^2 \\ \alpha^2 u^2 - \alpha^2 v_1^2 &= \alpha v_2^2 \\ \alpha^2 v_1^2 &= \alpha^2 u^2 - \alpha v_2^2\end{aligned}\quad (\text{D.8})$$

Combining [Equation \(D.7\)](#) and [Equation \(D.8\)](#) gives

$$\begin{aligned}\alpha^2 u^2 - 2\alpha u v_2 \cos \varphi + v_2^2 &= \alpha^2 u^2 - \alpha v_2^2 \\ v_2^2 + \alpha v_2^2 &= 2\alpha u v_2 \cos \varphi \\ v_2^2(1 + \alpha) &= 2\alpha u v_2 \cos \varphi \\ v_2 &= 2 \left(\frac{\alpha}{1 + \alpha} \right) u \cos \varphi\end{aligned}\quad (\text{D.9})$$

Substituting [Equation \(D.9\)](#) into [Equation \(D.8\)](#) we get

$$\begin{aligned}\alpha^2 v_1^2 &= \alpha^2 u^2 - \alpha \left(2 \left(\frac{\alpha}{1 + \alpha} \right) u \cos \varphi \right)^2 \\ v_1^2 &= u^2 - \frac{1}{\alpha} \left(4 \left(\frac{\alpha^2}{(1 + \alpha)^2} \right) u^2 \cos^2 \varphi \right) \\ v_1^2 &= u^2 \left(1 - 4 \left(\frac{\alpha}{(1 + \alpha)^2} \right) \cos^2 \varphi \right) \\ v_1 &= u \sqrt{1 - 4 \frac{\alpha}{M} \cos^2 \varphi}\end{aligned}\quad (\text{D.10})$$

where $\alpha/M = \alpha/(1 + \alpha)^2$. The ratio of [Equation \(D.3\)](#) and [Equation \(D.6\)](#) gives

$$\begin{aligned}\frac{\alpha v_1 \sin \theta}{\alpha v_1 \cos \theta} &= \frac{v_2 \sin \varphi}{\alpha u - v_2 \cos \varphi} \\ \tan \theta &= \frac{v_2 \sin \varphi}{\alpha u - v_2 \cos \varphi}\end{aligned}\quad (\text{D.11})$$

Inserting [Equation \(D.9\)](#) into [Equation \(D.11\)](#) gives

$$\begin{aligned}
 \tan \theta &= \frac{\left(2\left(\frac{\alpha}{1+\alpha}\right) u \cos \varphi\right) \sin \varphi}{\alpha u - \left(2\left(\frac{\alpha}{1+\alpha}\right) u \cos \varphi\right) \cos \varphi} \\
 \tan \theta &= \frac{\alpha u \left(\frac{1}{1+\alpha}\right) 2 \sin \varphi \cos \varphi}{\alpha u \left(1 - 2\left(\frac{1}{1+\alpha}\right) \cos^2 \varphi\right)} \\
 \tan \theta &= \frac{\sin 2\varphi}{\left(1 + \alpha\right) \left(1 - 2\left(\frac{1}{1+\alpha}\right) \cos^2 \varphi\right)} \\
 \tan \theta &= \frac{\sin 2\varphi}{1 + \alpha - 2 \cos^2 \varphi} \\
 \tan \theta &= \frac{\sin 2\varphi}{\alpha - (2 \cos^2 \varphi - 1)} \\
 \tan \theta &= \frac{\sin 2\varphi}{\alpha - \cos 2\varphi} \\
 \theta &= \arctan \left(\frac{\sin 2\varphi}{\alpha - \cos 2\varphi} \right)
 \end{aligned} \tag{D.12}$$

Substituting back the variable names from [Figure 2.1a](#) into [Equation \(D.12\)](#) gives

$$\theta_b = \arctan \left(\frac{\sin 2\theta_t}{\alpha - \cos 2\theta_t} \right) \tag{D.13}$$

D.2 Center of mass (CM) frame of reference

Using the same approach as [section D.1](#). From figure [Figure 2.1b](#) we can express the velocities as

$$\begin{aligned}
 \mathbf{u}'_1 &= u'_1 \hat{\mathbf{x}} \\
 \mathbf{u}'_2 &= u'_2 \hat{\mathbf{x}} \\
 \mathbf{v}'_b &= \mathbf{v}'_1 = v'_1 (\cos \theta' \hat{\mathbf{x}} + \sin \theta' \hat{\mathbf{y}}) \\
 \mathbf{v}'_t &= \mathbf{v}'_2 = v'_2 (-\cos \theta' \hat{\mathbf{x}} - \sin \theta' \hat{\mathbf{y}}) = -v'_2 (\cos \theta' \hat{\mathbf{x}} + \sin \theta' \hat{\mathbf{y}})
 \end{aligned} \tag{D.14}$$

where \mathbf{u}'_1 and \mathbf{v}'_1 is the initial and final velocity of the projectile $m_b = m_1$ respectively, and \mathbf{u}'_2 and \mathbf{v}'_2 is the initial and final velocity of the target $m_t = m_2$ respectively. The angle $\theta'_b = \theta'$ is the projectile angle.

In the center of mass (CM) frame of reference, the position of the center of mass is given by

$$\mathbf{R} = \frac{m_1 \mathbf{r}_1 + m_2 \mathbf{r}_2}{m_1 + m_2} \tag{D.15}$$

and the velocity is

$$\mathbf{V} = \frac{d\mathbf{R}}{dt} = \frac{d}{dt} \left(\frac{m_1 \mathbf{r}_1 + m_2 \mathbf{r}_2}{m_1 + m_2} \right) = \frac{m_1 \mathbf{u}'_1 + m_2 \mathbf{u}'_2}{m_1 + m_2} \quad (\text{D.16})$$

At the origin of the CM frame, $\mathbf{R} = 0$, which implies $\mathbf{V} = 0$. The total momentum before the collision is

$$\begin{aligned} m_1 \mathbf{u}'_1 + m_2 \mathbf{u}'_2 &= 0 \\ m_2 \mathbf{u}'_2 &= -m_1 \mathbf{u}'_1 \\ \mathbf{u}'_2 &= -\frac{m_1}{m_2} \mathbf{u}'_1 \\ \mathbf{u}'_2 &= -\alpha \mathbf{u}'_1 \end{aligned} \quad (\text{D.17})$$

and after the collision it is

$$\begin{aligned} m_1 \mathbf{v}'_1 + m_2 \mathbf{v}'_2 &= 0 \\ m_2 \mathbf{v}'_2 &= -m_1 \mathbf{v}'_1 \\ \mathbf{v}'_2 &= -\frac{m_1}{m_2} \mathbf{v}'_1 \\ \mathbf{v}'_2 &= -\alpha \mathbf{v}'_1 \\ -v'_2 (\cos \theta' \hat{\mathbf{x}} + \sin \theta' \hat{\mathbf{y}}) &= -\alpha v'_1 (\cos \theta' \hat{\mathbf{x}} + \sin \theta' \hat{\mathbf{y}}) \\ v'_2 &= \alpha v'_1 \end{aligned} \quad (\text{D.18})$$

Conservation of energy gives

$$\begin{aligned} \frac{1}{2} m_1 u'^2_1 + \frac{1}{2} m_2 u'^2_2 &= \frac{1}{2} m_1 v'^2_1 + \frac{1}{2} m_2 v'^2_2 \\ m_1 u'^2_1 + m_2 u'^2_2 &= m_1 v'^2_1 + m_2 v'^2_2 \end{aligned} \quad (\text{D.19})$$

Substituting Equation (D.17) and Equation (D.18) into Equation (D.19) gives

$$\begin{aligned} m_1 u'^2_1 + m_2 (-\alpha u'_1)^2 &= m_1 v'^2_1 + m_2 (\alpha v'_1)^2 \\ m_1 u'^2_1 + \alpha^2 m_2 u'^2_1 &= m_1 v'^2_1 + \alpha^2 m_2 v'^2_1 \\ (m_1 + \alpha^2 m_2) u'^2_1 &= (m_1 + \alpha^2 m_2) v'^2_1 \\ u'^2_1 &= v'^2_1 \\ u'_1 &= v'_1 \end{aligned} \quad (\text{D.20})$$

Substituting Equation (D.20) into Equation (D.17) gives

$$u'_2 = -\alpha v'_1 \quad (\text{D.21})$$

D.3 Connection between the LAB frame and the CM frame

Galilean transformations describes the relationship between the LAB frame and the CM frame

$$\begin{aligned} x' &= x - vt & v'_x &= v_x - V_{cm} \\ y' &= y & v'_y &= v_y \\ z' &= z & v'_z &= v_z \\ t' &= t \end{aligned}$$

Using the same approach as section D.1. In the LAB frame Figure 2.1a, conservation of momentum is given by

$$m_1 \mathbf{u}_1 + m_2 \mathbf{u}_2 = m_1 \mathbf{v}_1 + m_2 \mathbf{v}_2 = (m_1 + m_2) \mathbf{V} \quad (\text{D.22})$$

which can be written as

$$\begin{aligned} m_1 \mathbf{u}_1 + m_2 \mathbf{u}_2 &= (m_1 + m_2) \mathbf{V} \\ \mathbf{V} &= \frac{m_1 \mathbf{u}_1 + m_2 \mathbf{u}_2}{m_1 + m_2} & \mathbf{u}_2 &= 0 \\ \mathbf{V} &= \frac{m_1}{m_1 + m_2} \mathbf{u}_1 \\ \mathbf{V} &= \frac{\alpha}{1 + \alpha} u \hat{\mathbf{x}} \\ V &= \frac{\alpha}{1 + \alpha} u \end{aligned} \quad (\text{D.23})$$

Using Galilean transformations, the connection between \mathbf{v}'_1 and \mathbf{v}_1 is expressed as

$$\begin{aligned} \mathbf{v}'_1 &= \mathbf{v}_1 - \mathbf{V} \\ \mathbf{v}_1 &= \mathbf{v}'_1 + \mathbf{V} \end{aligned} \quad (\text{D.24})$$

which in x-direction gives

$$v_1 \cos \theta = v'_1 \cos \theta' + V \quad (\text{D.25})$$

and in y-direction gives

$$v_1 \sin \theta = v'_1 \sin \theta' \quad (\text{D.26})$$

The ratio of [Equation \(D.26\)](#) and [Equation \(D.25\)](#) gives

$$\begin{aligned}\frac{v_1 \sin \theta}{v_1 \cos \theta} &= \frac{v'_1 \sin \theta'}{v'_1 \cos \theta' + V} \\ \tan \theta &= \frac{\sin \theta'}{\cos \theta' + \frac{V}{v'_1}} \\ \tan \theta &= \frac{\sin \theta'}{\frac{V}{v'_1} + \cos \theta'}\end{aligned}\tag{D.27}$$

We need to reformulate the velocity ratio. Substitution from [Equation \(D.20\)](#) gives

$$\frac{V}{v'_1} = \frac{V}{u'_1}\tag{D.28}$$

Using Galilean transformation and [Equation \(D.23\)](#) we have that

$$\begin{aligned}\mathbf{u}'_1 &= \mathbf{u}_1 - \mathbf{V} \\ u'_1 &= u_1 - V \\ u'_1 &= u - \frac{\alpha}{1+\alpha}u \\ u'_1 &= u \left(1 - \frac{\alpha}{1+\alpha}\right) \\ u'_1 &= u \left(\frac{1+\alpha-\alpha}{1+\alpha}\right) \\ u'_1 &= \frac{1}{1+\alpha}u\end{aligned}\tag{D.29}$$

Substituting [Equation \(D.23\)](#) and [Equation \(D.29\)](#) into [Equation \(D.28\)](#) gives

$$\frac{V}{u'_1} = \frac{\frac{\alpha}{1+\alpha}u}{\frac{1}{1+\alpha}u} = \alpha\tag{D.30}$$

Substituting [Equation \(D.30\)](#) into [Equation \(D.27\)](#) gives

$$\begin{aligned}\tan \theta &= \frac{\sin \theta'}{\alpha + \cos \theta'} \\ \theta &= \arctan \left(\frac{\sin \theta'}{\alpha + \cos \theta'} \right)\end{aligned}\tag{D.31}$$

Substituting back the variable names from [Figure 2.1b](#) into [Equation \(D.31\)](#) gives

$$\theta_b = \arctan \left(\frac{\sin \theta'_b}{\alpha + \cos \theta'_b} \right) \quad (\text{D.32})$$

Using Galilean transformations, the connection between \mathbf{v}'_2 and \mathbf{v}_2 is expressed as

$$\begin{aligned} \mathbf{v}'_2 &= \mathbf{v}_2 - \mathbf{V} \\ \mathbf{v}_2 &= \mathbf{v}'_2 + \mathbf{V} \end{aligned} \quad (\text{D.33})$$

which in x-direction gives

$$\begin{aligned} v_2 \cos \varphi &= -v'_2 \cos \theta' + V \\ v_2 \cos \varphi &= V - v'_2 \cos \theta' \end{aligned} \quad (\text{D.34})$$

and in y-direction gives

$$v_2 \sin \varphi = v'_2 \sin \theta' \quad (\text{D.35})$$

The ratio of [Equation \(D.35\)](#) and [Equation \(D.34\)](#) gives

$$\begin{aligned} \frac{v_2 \sin \varphi}{v_2 \cos \varphi} &= \frac{v'_2 \sin \theta'}{V - v'_2 \cos \theta'} \\ \tan \varphi &= \frac{\sin \theta'}{\frac{V}{v'_2} - \cos \theta'} \end{aligned} \quad (\text{D.36})$$

We need to reformulate the velocity ratio. Substitution from [Equation \(D.18\)](#) and [Equation \(D.20\)](#) gives

$$\frac{V}{v'_2} = \frac{V}{\alpha v'_1} = \frac{V}{\alpha u'_1} \quad (\text{D.37})$$

Substituting [Equation \(D.30\)](#) into [Equation \(D.37\)](#) gives

$$\frac{V}{v'_2} = \frac{V}{\alpha \frac{V}{\alpha}} = 1 \quad (\text{D.38})$$

Substituting [Equation \(D.38\)](#) into [Equation \(D.36\)](#) gives

$$\begin{aligned}\tan \varphi &= \frac{\sin \theta'}{1 - \cos \theta'} = \frac{1}{\frac{1-\cos \theta'}{\sin \theta'}} = \frac{1}{\tan \frac{\theta'}{2}} = \cot \frac{\theta'}{2} \\ \varphi &= \frac{1}{2}(\pi - \theta') \text{ [radians]} = \frac{1}{2}(180^\circ - \theta') \text{ [degrees]}\end{aligned}\quad (\text{D.39})$$

Substituting back the variable names from [Figure 2.1](#) into [Equation \(D.39\)](#) gives

$$\theta_t = \frac{1}{2}(\pi - \theta'_b) \text{ [radians]} = \frac{1}{2}(180^\circ - \theta'_b) \text{ [degrees]} \quad (\text{D.40})$$

Appendix E

Connecting MiniballCoulexSort with ROOT

To connect MiniballCoulexSort with ROOT you need them to share their libraries with each other. This is done with a dynamic loader, which you can find out more about here [42].

You have to make a `.rootrc` file in your home folder on your computer. In the `.rootrc` file you want to write something like this

```
Unix.*.Root.DynamicPath:    .:/Users/trondwj/GitHub(ROOT-
framework/build/lib >:/Users/trondwj/GitHub/Miniball/
MiniballCoulexSort/lib :
```

This should all be in one line. The first part is to tell the system to use the dynamic loader of ROOT to connect the given paths that follow. In my case the lib folder of the ROOT install was at

```
/Users/trondwj/GitHub/ROOT-framework/build/lib
```

and the lib folder of the *MiniballCoulexSort* was at

```
/Users/trondwj/GitHub/Miniball/MiniballCoulexSort/lib
```

These paths are totally individual, and you will probably not have it in the same place. Therefore these paths must be changed to fit your system.

After making the file you either have restart the terminal or you can source the file by writing this in the terminal

```
$ source ~/.rootrc
```


Appendix F

Running ROOT and MiniballCoulexSort from anywhere in the terminal

To run ROOT or the different scripts of *MiniballCoulexSort* anywhere in the terminal, you have to edit your *.bash_profile* file [*.bash_profile* on MacOS, *.bashrc* on Linux]. In my *.bash_profile* I used this

```
# Run ROOT from anywhere
export ROOTSYS=$HOME/GitHub(ROOT-framework/build
export PATH=$ROOTSYS/lib:$PATH
export PATH=$ROOTSYS/bin:$PATH
export DYLD_LIBRARY_PATH=$ROOTSYS/lib:$DYLD_LIBRARY_PATH

# Run MiniballCoulexSort from anywhere
export DYLD_LIBRARY_PATH=$HOME/GitHub/Miniball/
    MiniballCoulexSort/lib:$DYLD_LIBRARY_PATH
export PATH=$HOME/GitHub/Miniball/MiniballCoulexSort/lib:$PATH
export PATH=$HOME/GitHub/Miniball/MiniballCoulexSort/bin:$PATH
```

The DYLD_LIBRARY_PATH is used on Mac only. On other systems, use LD_LIBRARY_PATH instead. You need to locate the *lib* and *bin* folders for both ROOT and *MiniballCoulexSort* and change them to fit your system, and in addition you need the build folder of your ROOT install.

Appendix G

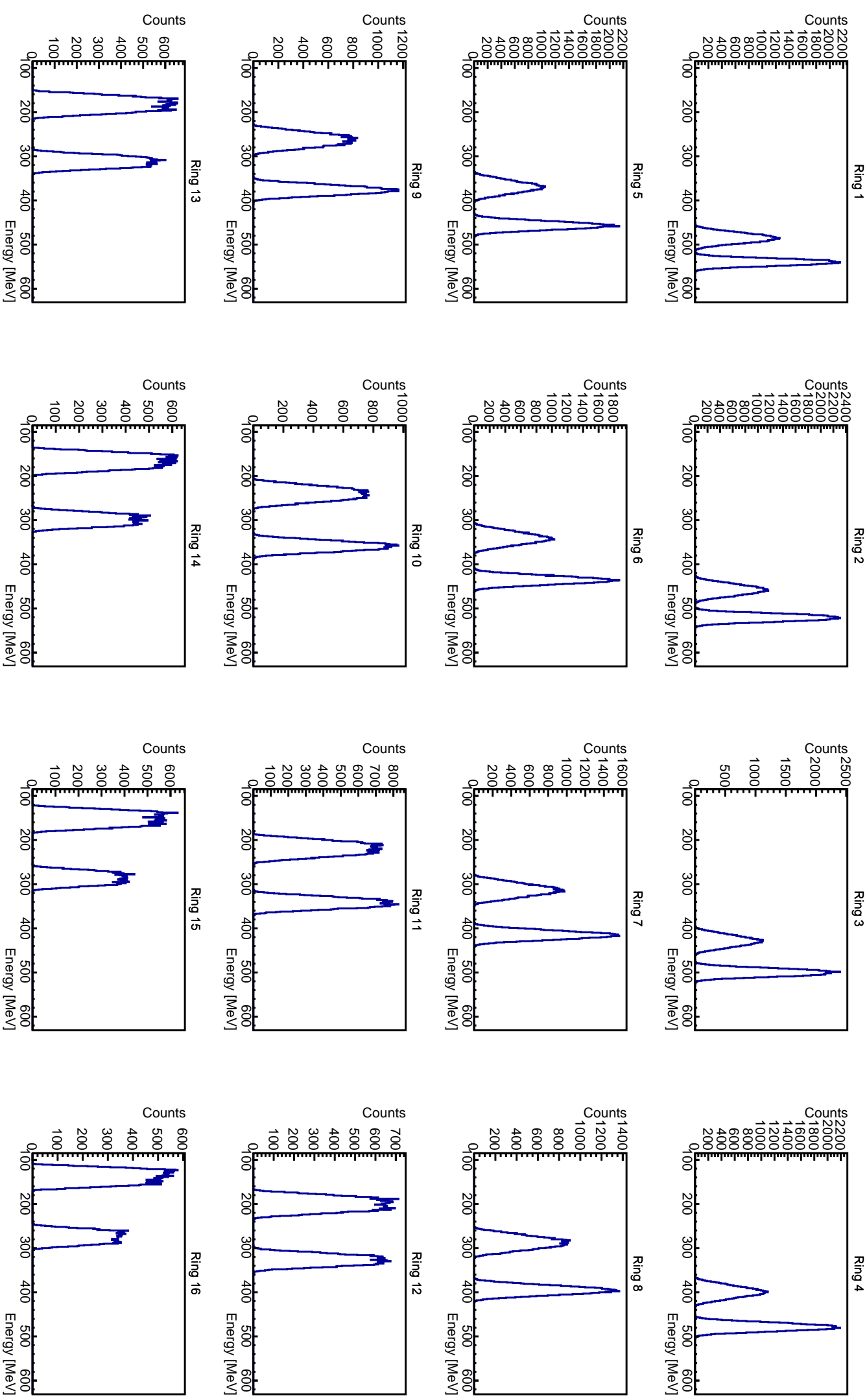
CD simulation

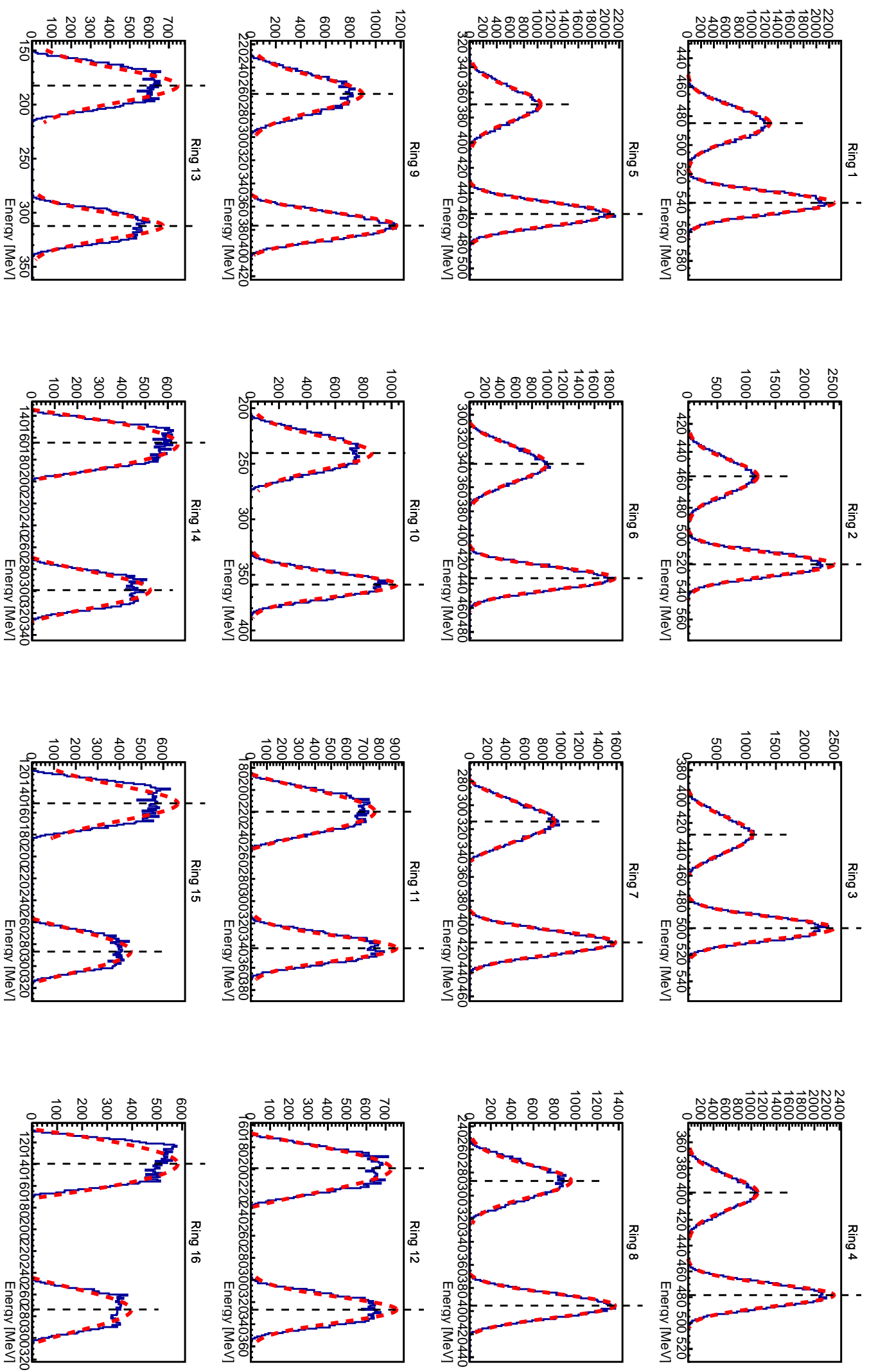
On the next page, the CD simulation is showed for each ring. Ring 1 is the innermost ring and ring 16 is the outermost ring. The plots show simulated counts vs. energy, where the first peak (lower energy) is the ^{208}Pb and the second peak (higher energy) is ^{140}Sm . The plots were grabbed from the `.root`-file by the commands

```
$ cd ~/GitHub/MasterThesis/Scripts/plotting
$ root
root [0] .L ParticlePlot.cpp++
root [1] simulation_plot("setup_Sm.txt", 0)
... <showing output from script>
```

The next page after that shows the fitting of the CD simulation, where the red dotted curves shows the fitting of the peaks and the vertical black dotted lines shows the centroids of the peaks.

```
$ cd ~/GitHub/MasterThesis/Scripts/fitting
$ root
root [0] .L ParticleFit.cpp++
root [1] simulation_fit("setup_Sm.txt")
... <showing output from script>
```





Bibliography

- [1] M. Klintefjord. *Evolution of deformation and collectivity away from magic numbers*. PhD thesis, University of Oslo, May 2016. URL <http://urn.nb.no/URN:NBN:no-56121>.
- [2] M. Klintefjord, K. Hadyńska-Klęk, J. Samorajczyk, et al. Spectroscopy of low-lying states in ^{140}Sm . *Acta Physica Polonica B*, 46(3):607–611, 2015. ISSN 0587-4254. doi: 10.5506/APhysPolB.46.607.
- [3] J. Samorajczyk, M. Klintefjord, C. Droste, et al. Revised spin values of the 991 keV and 1599 keV levels in Sm 140. *Physical Review C - Nuclear Physics*, 92(4):3–6, 2015. ISSN 1089490X. doi: 10.1103/PhysRevC.92.044322.
- [4] M. Klintefjord, K. Hadyńska-Klęk, A. Görgen, et al. Structure of low-lying states in Sm 140 studied by Coulomb excitation. *Physical Review C*, 93(5): 1–14, 2016. ISSN 24699993. doi: 10.1103/PhysRevC.93.054303.
- [5] NIST Physics Laboratory web site. URL <https://physics.nist.gov/constants>. Accessed: July 2019.
- [6] O. B. Tarasov and D. Bazin. Lise++: Radioactive beam production with in-flight separators. *Nuclear Instruments and Methods in Physics Research Section B: Beam Interactions with Materials and Atoms*, 266(19):4657 – 4664, 2008. ISSN 0168-583X. doi: <https://doi.org/10.1016/j.nimb.2008.05.110>. URL <http://lise.nscl.msu.edu/lise.html>. Proceedings of the XVth International Conference on Electromagnetic Isotope Separators and Techniques Related to their Applications.
- [7] P. Reiter, J. Eberth, H. Faust, et al. The MINIBALL array. *Nuclear Physics A*, 701(1-4):209–212, 2002. ISSN 03759474. doi: 10.1016/S0375-9474(01)01576-7.
- [8] M. J. Borge and K. Riisager. HIE-ISOLDE, the project and the physics opportunities. *European Physical Journal A*, 52(11), 2016. ISSN 1434601X. doi: 10.1140/epja/i2016-16334-4.

- [9] The ISOLDE web page. URL <http://isolate.web.cern.ch>. Accessed: July 2019.
- [10] B. Jonson and K. Riisager. The ISOLDE facility. *Scholarpedia*, 5(7):9742, 2010. doi: 10.4249/scholarpedia.9742. Revision #90796.
- [11] Nucleonica Newsletter, 2019. URL <https://www.nucleonica.com/wiki/images/c/cb/NucleonicaNewsletter2019.pdf>. Accessed: July 2019.
- [12] D. Olsen. First generation ISOL radioactive ion beam facilities. pages 312–316, 2002. doi: 10.1109/pac.1995.504646.
- [13] N. Warr, J. Van de Walle, M. Albers, et al. The miniball spectrometer. *European Physical Journal A*, 49(3):1–32, 2013. ISSN 1434601X. doi: 10.1140/epja/i2013-13040-9.
- [14] C. Lefèvre. The CERN accelerator complex. Complexe des accélérateurs du CERN. Dec 2008. URL <https://cds.cern.ch/record/1260465>.
- [15] R. Catherall, W. Andreadza, M. Breitenfeldt, et al. The ISOLDE facility. 2, 2017. ISSN 13616471. doi: 10.1088/1361-6471/aa7eba.
- [16] M. J. Borge. The ISOLDE facility: Recent highlights and the HIE-ISOLDE project. *Proceedings of Science*, 11005:1–8, 2013. ISSN 18248039.
- [17] The ISOLDE RILIS web page. URL <http://rilis.web.cern.ch>. Accessed: July 2019.
- [18] B. A. Marsh, B. Andel, A. N. Andreyev, et al. New developments of the in-source spectroscopy method at RILIS/ISOLDE. *Nuclear Instruments and Methods in Physics Research, Section B: Beam Interactions with Materials and Atoms*, 317(PART B):550–556, 2013. ISSN 0168583X. doi: 10.1016/j.nimb.2013.07.070. URL <http://dx.doi.org/10.1016/j.nimb.2013.07.070>.
- [19] T. D. Goodacre, V. Fedossev, S. Rothe, et al. Ion beam production and study of radioactive isotopes with the laser ion source at ISOLDE. *Journal of Physics G: Nuclear and Particle Physics*, 44(8):084006, 2017. ISSN 0954-3899. doi: 10.1088/1361-6471/aa78e0.
- [20] E. Kugler, D. Fiander, B. Johnson, et al. The new CERN-ISOLDE on-line mass-separator facility at the PS-Booster. *Nuclear Inst. and Methods in Physics Research, B*, 70(1-4):41–49, 1992. ISSN 0168583X. doi: 10.1016/0168-583X(92)95907-9.
- [21] P. Schmidt, F. Ames, G. Bollen, et al. Bunching and cooling of radioactive ions with REXTRAP. *Nuclear Physics A*, 701(1-4):550–556, 2002. ISSN 03759474. doi: 10.1016/S0375-9474(01)01642-6.

- [22] F. Ames, G. Bollen, P. Delahaye, et al. Cooling of radioactive ions with the Penning trap REXTRAP. *Nuclear Instruments and Methods in Physics Research, Section A: Accelerators, Spectrometers, Detectors and Associated Equipment*, 538(1-3):17–32, 2005. ISSN 01689002. doi: 10.1016/j.nima.2004.08.119.
- [23] B. H. Wolf, J. Cederkäll, O. Forstner, et al. First radioactive ions charge bred in REXEBIS at the REX-ISOLDE accelerator. *Nuclear Instruments and Methods in Physics Research, Section B: Beam Interactions with Materials and Atoms*, 204:428–432, 2003. ISSN 0168583X. doi: 10.1016/S0168-583X(02)02108-0.
- [24] Y. Kadi, Y. Blumenfeld, W. V. Delsolaro, et al. Post-accelerated beams at ISOLDE. *Journal of Physics G: Nuclear and Particle Physics*, 44(8), 2017. ISSN 13616471. doi: 10.1088/1361-6471/aa78ca.
- [25] The REX-ISOLDE web page. URL <http://rex-isolde.web.cern.ch>. Accessed: July 2019.
- [26] The HIE-ISOLDE web page. URL <http://hie-isolde-project.web.cern.ch>. Accessed: July 2019.
- [27] F. Wenander. EBIS as charge breeder for radioactive ion beam accelerators. *Nuclear Physics A*, 701(1-4):528–536, 2002. ISSN 03759474. doi: 10.1016/S0375-9474(01)01640-2.
- [28] F. Wenander. Charge breeding of radioactive ions with EBIS and EBIT. *Journal of Instrumentation*, 5(10), 2010. ISSN 17480221. doi: 10.1088/1748-0221/5/10/C10004.
- [29] F. L. Bello Garrote, A. Görgen, J. Mierzejewski, et al. Lifetime measurement for the 21+ state in Sm 140 and the onset of collectivity in neutron-deficient Sm isotopes. *Physical Review C - Nuclear Physics*, 92(2):1–8, 2015. ISSN 1089490X. doi: 10.1103/PhysRevC.92.024317.
- [30] N. Warr. *The Miniball double-sided silicon strip detector (CD)*, October 2015. URL <https://www.ikp.uni-koeln.de/~warr/doc/cd.pdf>. Accessed: April 2019.
- [31] A. N. Ostrowski, S. Cherubini, T. Davinson, et al. CD: A double sided silicon strip detector for radioactive nuclear beam experiments. *Nuclear Instruments and Methods in Physics Research, Section A: Accelerators, Spectrometers, Detectors and Associated Equipment*, 480(2-3):448–455, 2002. ISSN 01689002. doi: 10.1016/S0168-9002(01)00954-8.

- [32] N. Warr. *The Miniball Cluster*, March 2005. URL https://www.ikp.uni-koeln.de/~warr/doc/miniball_detectors.pdf. Accessed: July 2019.
- [33] P. A. Butler, J. Cederkall, and P. Reiter. Nuclear-structure studies of exotic nuclei with MINIBALL. *Journal of Physics G: Nuclear and Particle Physics*, 44(4), 2017. ISSN 1361-6471. doi: 10.1088/1361-6471/aa5c4e.
- [34] R. Lutter, O. Schaile, K. Schoffel, et al. MARaBOOU-A MBS and ROOT based online/offline utility. *SANTA FE 1999 - 11th IEEE NPSS Real Time Conference, Conference Record, RT 1999*, (May):363–366, 1999. doi: 10.1109/RTCON.1999.842643.
- [35] H. G. Essel and N. Kurz. The general purpose data acquisition system MBS. *SANTA FE 1999 - 11th IEEE NPSS Real Time Conference, Conference Record, RT 1999*, 41(2):475–478, 1999. doi: 10.1109/RTCON.1999.842672.
- [36] R. Brun and F. Rademakers. ROOT - An Object Oriented Data Analysis Framework. Proceedings AIHENP’96 Workshop, Lausanne, Sep. 1996, Nucl. Inst. & Meth. in Phys. Res. A 389 (1997) 81-86, . URL <https://github.com/root-project/root>. doi: 10.5281/zenodo.2557526. Download: December 2018.
- [37] Analysis code for MINIBALL experiments at ISOLDE. URL <https://github.com/Miniball/MiniballCoulexSort>. doi: 10.5281/zenodo.2593370. Download: March 2019.
- [38] W. R. Leo. *Techniques for Nuclear and Particle Physics Experiments*. Springer, Berlin, Heidelberg, second revised edition, 1994. doi: 10.1007/978-3-642-57920-2.
- [39] L. Gaffney. Kinematics simulations for Coulomb-excitation experiments at Miniball. URL <https://github.com/lpgaff/kinsim>. Download: May 2018.
- [40] J. F. Ziegler, J. P. Biersack, and M. D. Ziegler. SRIM - The Stopping and Range of Ions in Matter, 2013. URL <http://www.srim.org>. Download: February 2018.
- [41] N. Warr. *Miniball Flexible Frame*, March 2015. URL <https://www.ikp.uni-koeln.de/~warr/doc/frame.pdf>. Accessed: July 2019.
- [42] R. Brun and F. Rademakers. ROOT - User’s Guide, . URL <https://root.cern.ch/root/html/doc/guides/users-guide/ROOTUsersGuide.html#file-system.rootrc>. Accessed: August 2019.